ARTICLE

Neuron-Derived Neurotrophic Factor Is Mutated in Congenital Hypogonadotropic Hypogonadism

Andrea Messina,[1,11] Kristiina Pulli,[2,11] Sara Santini,[1,11] James Acierno,[1,9] Johanna Känsäkoski,[3] Daniele Cassatella,[1,9] Cheng Xu,[1] Filippo Casoni,[4,8,9] Samuel A. Malone,[4] Gaetan Ternier,[4] Daniele Conte,[5] Yisrael Sidis,[1] Johanna Tommiska,[3] Kirsi Vaaralahti,[2] Andrew Dwyer,[1] Yoav Gothilf,[6] Giorgio R. Merlo,[5] Federico Santoni,[1] Nicolas J. Niederländer,[1] Paolo Giacobini,[4,12] Taneli Raivio,[2,7,12] and Nelly Pitteloud[1,10,12,*]

Congenital hypogonadotropic hypogonadism (CHH) is a rare genetic disorder characterized by infertility and the absence of puberty. Defects in GnRH neuron migration or altered GnRH secretion and/or action lead to a severe gonadotropin-releasing hormone (GnRH) deficiency. Given the close developmental association of GnRH neurons with the olfactory primary axons, CHH is often associated with anosmia or hyposmia, in which case it is defined as Kallmann syndrome (KS). The genetics of CHH are heterogeneous, and >40 genes are involved either alone or in combination. Several CHH-related genes controlling GnRH ontogeny encode proteins containing fibronectin-3 (FN3) domains, which are important for brain and neural development. Therefore, we hypothesized that defects in other FN3-superfamily genes would underlie CHH. Next-generation sequencing was performed for 240 CHH unrelated probands and filtered for rare, protein-truncating variants (PTVs) in FN3-superfamily genes. Compared to gnomAD controls the CHH cohort was statistically enriched for PTVs in neuron-derived neurotrophic factor (*NDNF*) ($p = 1.40 \times 10^{-6}$). Three heterozygous PTVs (p.Lys62*, p.Tyr128Thrfs*55, and p.Trp469*, all absent from the gnomAD database) and an additional heterozygous missense mutation (p.Thr201Ser) were found in four KS probands. Notably, NDNF is expressed along the GnRH neuron migratory route in both mouse embryos and human fetuses and enhances GnRH neuron migration. Further, knock down of the zebrafish ortholog of *NDNF* resulted in altered GnRH migration. Finally, mice lacking *Ndnf* showed delayed GnRH neuron migration and altered olfactory axonal projections to the olfactory bulb; both results are consistent with a role of *NDNF* in GnRH neuron development. Altogether, our results highlight *NDNF* as a gene involved in the GnRH neuron migration implicated in KS.

Introduction

Congenital hypogonadotropic hypogonadism (CHH [MIM: 146110, MIM: 147950, MIM: 228300, MIM: 229070, MIM: 244200, MIM: 308700, MIM: 610628, MIM: 612370, MIM: 612702, MIM: 614837, MIM: 614838, MIM: 614839, MIM: 614840, MIM: 614841, MIM: 614842, MIM: 614858, MIM: 614880, MIM: 614897, MIM: 615266, MIM: 615267, MIM: 615269, MIM: 615270, MIM: 615271, and MIM: 616030]) is characterized by infertility and the absence of puberty. It is a rare genetic disorder caused by absent secretion or action of gonadotropin-releasing hormone (GnRH) and is often associated with non-reproductive phenotypes. The most commonly associated phenotype is anosmia, which when combined with CHH is defined as Kallmann syndrome (KS [MIM: 308700, MIM: 614897, and MIM: 613301). However, synkinesia, unilateral renal agenesis, sensorineural deafness, cleft palate, and other phenotypes are also observed.[1,2]

The genetics of CHH are complex, and mutations are described in more than 40[1,2] genes. Variable expressivity both within and between families, as well as incomplete penetrance, is often present.[1,2] Although first described as a Mendelian disorder, both monogenic and oligogenic inheritance (i.e., mutations in more than one gene) occur in CHH.[1–3] However, in approximately 50% of affected individuals, no mutations could be identified in the known CHH genes.[3]

To date, the genes implicated in CHH impact GnRH neuron fate, GnRH neuron migration and/or axon projection, GnRH neuron homeostasis, and/or gonadotrope defects. Notably, a unique feature of GnRH neurons is that they originate in the olfactory placode during embryonic development and migrate along the terminal nerve to reach their final destination in the hypothalamus.[4–6] This complex migratory process is orchestrated by an intricate network of genes controlling cell signaling, adhesion, motility, and neurite and axonal elongation.

[1]Service of Endocrinology, Diabetology, and Metabolism, Lausanne University Hospital, 1011 Lausanne, Switzerland; [2]Stem Cells and Metabolism Research Program, Faculty of Medicine, University of Helsinki, 00014 Helsinki, Finland; [3]Department of Physiology, Faculty of Medicine, University of Helsinki, 00014 Helsinki, Finland; [4]Inserm, Jean-Pierre Aubert Research Center, Development and Plasticity of the Neuroendocrine Brain, Unité 1172 Lille, 59045 Lille, France; [5]Department of Molecular Biotechnology and Health Science, University of Torino, 10126 Torino, Italy; [6]Department of Neurobiology, George S. Wise Faculty of Life Sciences and Sagol School of Neurosciences, University of Tel Aviv, Tel Aviv 69978, Israel; [7]Pediatric Research Center, New Children's Hospital, Helsinki University Hospital, 00290 Helsinki, Finland; [8]Division of Neuroscience, San Raffaele Scientific Institute, Milan 20132, Italy, Milan 20132, Italy; [9]Università Vita-Salute San Raffaele, Via Olgettina 58, 20132, Milan, Italy; [10]Faculty of Biology and Medicine, University of Lausanne, Lausanne 1005, Switzerland
[11]These authors contributed equally to this work
[12]These authors contributed equally to this work
*Correspondence: nelly.pitteloud@chuv.ch
https://doi.org/10.1016/j.ajhg.2019.12.003.

ANOS1 (formerly known as *KAL1* [MIM: 300836]) was the first gene implicated in KS.[7,8] *ANOS1* encodes anosmin-1, which belongs to the fibronectin-3 (FN3) superfamily. Members of this family also include extracellular-matrix molecules and cell-surface hormone and cytokine receptors,[9] and the evolutionarily conserved FN3 domain is typically involved in protein-protein interactions related to cell adhesion, migration, and embryonic development.[10] Notably, mutations in several additional genes within this family have been associated with CHH; such genes include *AXL* [MIM: 109135], *FLRT3* [MIM: 604808], *LEPR* [MIM: 601007], and most recently, *DCC* [MIM: 120470].[2] Thus, we hypothesized that other proteins containing FN3 domains would also be involved in GnRH neuron ontogeny and contribute to the pathogenesis of CHH. Through a gene-based burden analysis of FN3-superfamily genes, we identified *NDNF*—a neurotrophic factor involved in neuron survival, migration, and neurite outgrowth[11]—as a locus for CHH.

Subjects and Methods

Subjects

A total of 240 unrelated CHH probands (140 KS and 100 normosmic CHH [nCHH], 179 males and 61 females) were included in the study. 222 individuals were from the Centre Hospitalier Universitaire Vaudois, and 85% were of European descent. The remaining 18 were from the Helsinki University Hospital and were of Finnish origin (See Supplemental Material and Methods). Diagnoses of nCHH and KS were made as previously described,[1,12,13] and family members were recruited when possible. All subjects provided written informed consent, and the study was approved by the institutional ethics committee at the University of Lausanne and the Helsinki University Central Hospital.

DNA Sequencing and Bioinformatic Analyses

Genomic DNA was extracted from peripheral blood (or saliva) through the use of commercially available QIAGEN kits according to the manufacturer's protocol. Whole-exome sequencing (WES), alignment, and variant calling were performed as previously described.[14,15] All variants were then annotated with minor-allele frequencies (MAFs) from gnomAD (see Supplemental Material and Methods for details). Protein-truncating variants (PTVs; defined as stop gain, frameshift, and acceptor-donor splice sites ± 2 bp from the exon) with MAF ≤ 0.1% were identified in the 204 FN3-superfamily genes obtained from the Interpro database (IPR003961, see Table S1). A gene-based burden analysis for the FN3-superfamily genes was performed with a two-tailed Fisher's exact test in CHH probands versus controls (gnomAD). To correct for multiple testing, we set a significance threshold at $p < 2.45 \times 10^{-4}$. Candidate FN3 genes were then prioritized according to the following criteria: (1) a significant enrichment of mutations in the CHH cohort as assessed with the gene-based burden test[16] and (2) mutations in FN3 candidate genes that are present in individuals for whom the CHH genes do not contain any mutations that would fully explain their phenotype (see Supplemental Material and Methods). All variants in *NDNF* were confirmed with bi-directional Sanger sequencing.

Cell-Based Functional Assays

NDNF Protein Expression and Cell-Surface Expression

A double FLAG tag was added to the N terminus of human *NDNF* (GenBank: NM_024574.3) in the pCDNA3.1 expression plasmid. We used site-directed mutagenesis to introduce the mutations into the construct by using a QuickChange II Site-Directed Mutagenesis Kit (Stratagene) according to the manufacturer's protocol. To assess the impact of the mutants on the expression and secretion of NDNF, we performed western-blot and cell-surface expression assays as previously described.[14,17]

Reporter Gene Assay

We used a nuclear factor of activated T cells (NFAT)-luciferase-based reporter bioassay to assess the activity of the wild-type (WT) and mutant NDNF in COS7 cells treated with increasing doses of FGF8 (addgene plasmid 10959).[18,19] NFAT is a reporter for the PLCγ/Ca^{+2} cascade downstream of FGF8/FGFR1 signaling (see Supplemental Material and Methods).

Recombinant NDNF Protein Production

Full-length untagged 568 amino acid recombinant human NDNF protein (Uniprot: Q8TB73) was produced with the QMCF stable episomal expression system after cDNA codon optimization was performed in CHO cells by Icosagen (see Supplemental Material and Methods).

Cell-Culture and Migration Assays

Transwell experiments were performed with the GN11 cell line as previously reported.[20] In brief, GN11 cells were seeded on the upper side of 8-mm-pore filters in transwell chambers and incubated for 8 h in 10% fetal bovine serum (FBS) DMEM with or without recombinant NDNF (10, 100, 200, 500 ng/mL; Icosagen). rNDNF was added either to both chambers (n = 5 for each dose) or only in the upper chamber (n = 5 for each dose). GN11 cells that migrated to the lower side of the filter were then fixed in cold 100% methanol for 5 min, and the nuclei were stained with DAPI for subsequent quantitative analysis. Data were compared by one-way ANOVA for multiple comparisons.

We performed three-dimensional matrix migration assays by co-culturing aggregates of GN11 cells with aggregates of COS7 cells[21] transfected with plasmids encoding either mutated NDNF or WT NDNF as a control. We created cell aggregates by resuspending GN11 and COS7 cells in 2 μL or 5 μL of growth-factor-free Matrigel (BD Biosciences; 10^6 cells/mL), respectively, placing them on a culture dish, and inverting them until the gel had set. The droplets were then covered with a growth-factor-reduced Matrigel coating and kept in culture for 72 h. For analysis, the aggregates were fixed with paraformaldehyde (PFA) 4% for 40 min and stained with Alexa Fluor 594 Phalloidin (Invitrogen) for 30 min at room temperature. Photographs were taken for quantitative analysis with ImageJ. For illustration, photomicrographs have been digitally inverted, and a pseudo-color (purple) has been superimposed so that the cell distribution is highlighted.

Zebrafish Experiments

Animal Model

We used the *OMP^{2k}:gap-CFP^{rw034}* and *TRPC2$^{4.5k}$:gap-Venus^{rw037}* transgenic zebrafish strains[22–24] as reporters to visualize, respectively, the OMP+ and the Trpc2+ neurons and their axonal projections of the zebrafish olfactory system during embryonic development, as previously described.[25] We used the *GnRH3::GFP* strain to visualize the zebrafish GnRH3+ neurons.[25,26] A conventional antisense morpholino oligo (MO)-mediated strategy was used for down-modulation of *z-ndnf*.[27,28] This involved two previously validated anti-*z-ndnf* MOs—one targeting the splice junction

between intron 3 and exon 4 and leading to a premature stop codon upstream of the homeodomain and a second that anneals to the ATG start codon and prevents translation.[29] As a control, a sequence previously shown to have no effect was used.[30] Zebrafish embryos were injected at the one-cell stage with 4 ng of control or anti-*z-ndnf* MO, and then the number, morphology, and position relative to the olfactory placode of GFP+ cells in the frontonasal piece were examined at 72 hours post-fertilization (hpf), as previously described.[25,30]

Real-Time qPCR Analysis for Coding mRNAs

Relative mRNA levels of *z-OMPa, z-OMPb, z-Trpc2*, and *z-HoxA10b* were determined by real-time qPCR in total RNA samples extracted from the heads of *z-ndnf*- or control-MO injected zebrafish embryos, as previously described.[25] The abundance of *z-β actin* mRNAs was used for normalization because doing so was previously shown to be the best method.[31] The Roche UPS online tool was used for primer design (Supplemental Material and Methods), and the ΔΔCt formula (ABI software version 2.1, Applied Biosystems) was used for data analysis.[25]

Expression Studies in Mice

Mouse Model

GnRH-GFP[32] mice were graciously provided by Dr. Daniel J. Spergel (Section of Endocrinology, Department of Medicine, University of Chicago). Mice were housed under specific pathogen-free conditions in a temperature-controlled room (21°C –22°C) with a 12 h light/dark cycle and *ad libitum* access to food and water. Animal studies were approved by the Institutional Ethics Committees of Care and Use of Experimental Animals of the University of Lille 2. All experiments were performed in accordance with the guidelines for animal use specified by the European Union Council Directive of September 22, 2010 (2010/63/EU).

Fluorescence-Activated Cell Sorting and Gene-Expression Analysis

GnRH-GFP neurons were isolated from embryos at embryonic days 14.5 and 18.5 (E14.5 and E18.5) through the use of a previously validated fluorescence-activated cell sorting (FACS) protocol.[33] Reverse transcription and linear pre-amplification were performed, and *Ndnf* expression was measured by qRT PCR with Taqman expression assays. Data were compared by one-way ANOVA for multiple comparisons and a subsequent Tukey's least-significant-difference post-hoc test. A detailed description is provided in the Supplemental Material and Methods.

Collection and Processing of Human Fetuses

Tissues were made available in accordance with French bylaws (*Good Practice Concerning the Conservation, Transformation, and Transportation of Human Tissue to Be Used Therapeutically*, published on December 29, 1998). The studies on human fetal tissue were approved by the French agency for biomedical research (Agence de la Biomédecine, Saint-Denis la Plaine, France, protocol n°: PFS16–002). Non-pathological human fetuses (7 and 11 gestational weeks (GW), n = 3) were obtained from voluntarily terminated pregnancies after written informed consent was obtained from the parents (Gynaecology Department, Jeanne de Flandre Hospital, Lille, France). Fetuses were fixed by immersion in 4% PFA at 4°C for 5 days. The tissues were then cryoprotected in PBS containing 30% sucrose at 4°C overnight, embedded in Tissue-Tek OCT compound (Sakura Finetek), frozen in dry ice, and stored at −80°C until sectioning. Frozen samples were cut serially at 20 μm with a Leica CM 3050S cryostat (Leica Biosystems Nussloch GmbH) and immunolabeled, as described above and as previously described,[34,35] with the following primary antibodies: guinea pig anti-GnRH (dilution 1:10000), a kind gift from Erik Hrabovszky (Institute of Experimental Medicine, University of Budapest); monoclonal mouse TUJ1 (Sigma, 1:1000); and rabbit polyclonal NDNF (1:200; Cat: ARP68872_P050, Aviva Systems Biology).

Ndnf Knockout Mice

A *Ndnf* knockout (KO) mouse strain on the C57BL/6N genetic background was obtained from a NorCOMM B6N-derived C2 ES cell line generated by Geoffrey Hicks at the University of Manitoba (NorCOMM design ID N02206). Most of the coding part of *Ndnf* was deleted by homologous recombination. The targeting cassette replaced part of intron 3, the coding sequence of exon 4, and part of the 3′ UTR of the gene with an *E. coli* lacZ reporter construct, thus resulting in a non-functional gene product. Microinjections and production of KO mice were carried out at the Biocenter Oulu Transgenic Core Facility. Genotyping of the mice was performed as described in the Supplemental Material and Methods. The mice were housed with a 12 h light/dark cycle and *ad libitum* access to food and water. Both heterozygous and homozygous *Ndnf* KO mice appeared grossly normal and were able to produce viable pups.

All experiments were performed according to the guidelines for animal experiments at the University of Helsinki and under a license from the Finnish Review Board for Animal Experiments.

iDISCO Whole-Mount Staining

Experiments were performed as previously described[36] and are detailed in Supplemental Material and Methods.

GnRH Cell Counting

Embryos were harvested at embryonic day 13.5 from *Ndnf* transgenic mice (wild-type, n = 5; heterozygous, n = 7; and homozygous, n = 4). Heads from the embryos were washed thoroughly in cold 0.01 M PBS, preserved in fixative solution (4% PFA, 0.01 M PBS [pH 7.4]] for 6–8 h at 4°C, and immunolabelled for GnRH and peripherin through the use of iDISCO as described above. Primary antibodies used for these experiments were guinea pig anti-GnRH (dilution 1:10000), which was a kind gift from Erik Hrabovszky (Institute of Experimental Medicine, University of Budapest) and rabbit polyclonal anti-peripherin (Millipore, 1:1000). Quantitative analysis of GnRH neuronal number and location was performed over four regions: nose, olfactory bulb, ventral forebrain, and cortex. Both coronal and sagittal views were used for confirming accurate GnRH neuron localization, and counting was performed every 20 planes on the 4× zoom tiff series with Fiji and the Cell Counter plug-in.

Statistical Analysis

Sample sizes for neuroanatomical studies, gene expression, and *in vitro* motility analyses were estimated on the basis of prior experience and similar published studies. For the mouse work, typically, embryos taken from at least two different litters for each group were used.

Quantitative RT-PCR gene-expression data were analyzed with SDS 2.4.1 and Data Assist 3.0.1 software (Applied Biosystems). All other analyses were performed with Prism 5 (GraphPad software). Datasets were assessed for normality (Shapiro-Wilk test) and variance. When appropriate, a one-way ANOVA followed by Bonferroni or Dunnets's post-hoc correction was performed as indicated in the figure legends. Exact p values and adjusted

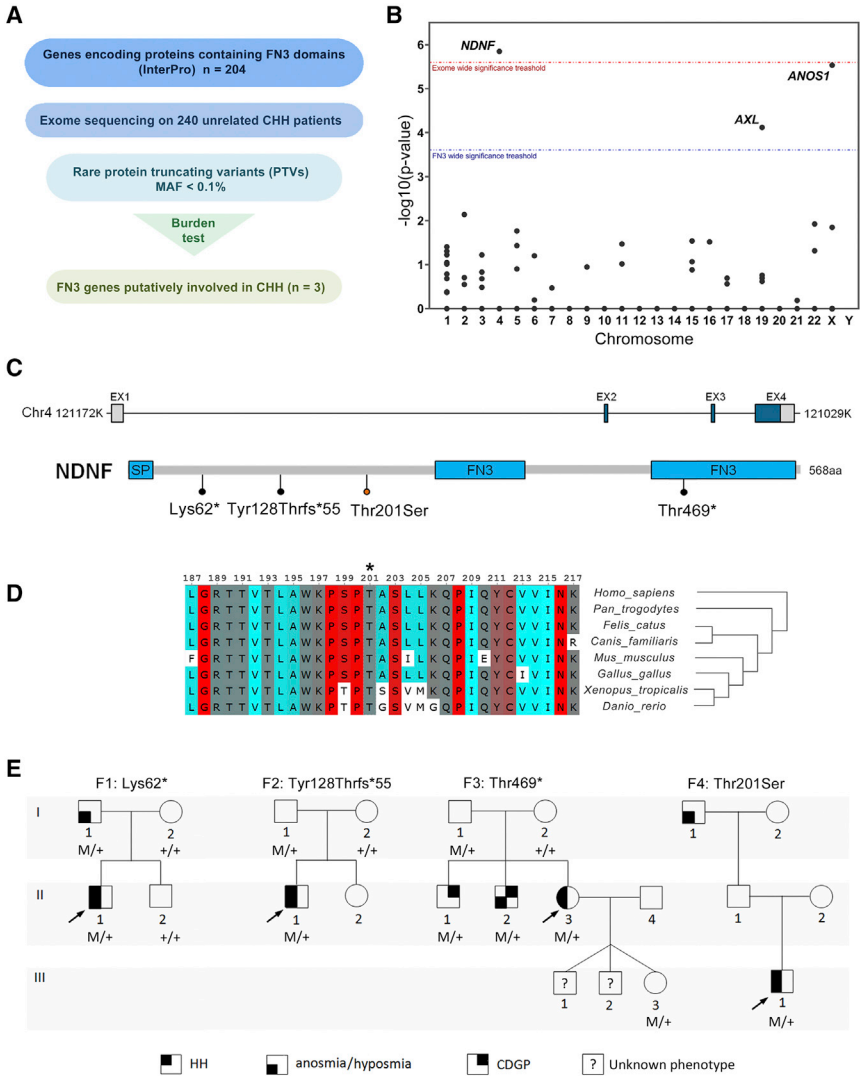

Figure 1. Exome Sequencing Identifies *NDNF* Mutations in KS Patients

(A) Filtering strategy for identifying novel candidate CHH-related genes.

(B) Manhattan plot of gene-based burden testing for FN3-superfamily genes. The red and blue dotted lines indicate the threshold for statistical significance after correction for multiple testing (red: n = 20,000, $p < 2.5 \times 10^{-6}$; blue: n = 204, $p < 2.45 \times 10^{-4}$).

(C) Schematic depiction of *NDNF* mRNA and protein; identified mutations are indicated. SP, signal peptide; FN3, fibronectin type 3 domain.

(D) Alignment of partial protein sequences of *NDNF* orthologs shows that the p.Thr201Ser mutation (asterisk) affects evolutionarily conserved amino acid residues across vertebrates (colored highlighting, turn propensity).

(E) Pedigrees of four families harboring *NDNF* mutations. Phenotypes are indicated by hatched symbols as shown in the legend (bottom), and arrows indicate the probands. HH, hypogonadotropic hypogonadism; CDGP, congenital delay of growth and puberty.

p values are given in the figure legends where possible. α was set at 0.05 for all experiments except where otherwise specified.

Results

Gene-Based Burden Testing Identifies Neuron-Derived Neurotrophic Factor as a Putative CHH-Associated Gene

Given that several CHH-associated genes encode proteins containing FN3 domains, WES data from 240 unselected CHH-affected individuals (143 KS and 97 normosmic CHH) were filtered for rare (MAF < 0.1% in gnomAD) PTVs in the 204 FN3-superfamily genes from the Interpro database (Table S1). Next, a gene-based burden analysis comparing the frequency of PTVs in affected individuals to that of individuals in the gnomAD control database was performed. A statistical enrichment for PTVs in CHH-affected probands was demonstrated for three FN3 genes (Figures 1A and 1B), including two known CHH-associated genes (*ANOS1*, $p = 2.88 \times 10^{-6}$; *AXL*, $p = 7.46 \times 10^{-5}$) and one novel gene, *NDNF* [MIM: 616506] ($p = 1.40 \times 10^{-6}$). Notably, none of the probands carrying *NDNF* PTVs had mutations in the known CHH-affected genes.

Individuals with KS Harbor NDNF Mutations

In addition to the three heterozygous PTVs identified in CHH probands in the burden analysis (GenBank: NM_024574.3; c.184A>T [p.Lys62*], c.381del [p.Tyr128Thrfs*55], c.1406G>A [p.Trp469*]), we identified one additional heterozygous missense mutation (c.602C>G [p.Thr201Ser]) predicted to be deleterious in 4/6 programs (PolyPhen-2, MutationTaster, LRT, and CADD).

The genetic and clinical information of the probands harboring *NDNF* mutations is summarized in Table 1 and Figure 1E. Notably, all four probands exhibit severe GnRH deficiency and anosmia (related to KS). In addition to prepubertal testes, the male probands had cryptorchidism and micropenis, suggesting an abnormal GnRH activation during mini-puberty.[2] The female proband presented with primary amenorrhea at age 17 (see the Supplemental Information for a description of affected individuals). Furthermore, three of these probands' family members (F1:I,1; F3:II,1; and F3:II,2) also carry *NDNF* mutations and have partial phenotypes (i.e., anosmia or constitutional delay of puberty), suggesting an autosomal-dominant inheritance with variable expressivity (Figure 1E). The presence of asymptomatic carriers (F2:I,1; F3:I,1; and F3:III,3) is consistent with incomplete penetrance.

Table 1. Phenotype and Genotype of Four Probands with Heterozygous NDNF Mutations

Subject	Sex	NDNF Mutation	MAF	Diagnosis	Inheritance	Other Phenotypes
F1:II,1	M	p.Lys62*	absent	KS	familial	micropenis crytorchidism
F2: II,1	M	p.Tyr128Thrfs*55	absent	KS	sporadic	cryptorchidism
F2:II,3	F	p.Trp469*	absent	KS	familial	
F3:III,1	M	p.Thr201Ser	0.10%	KS	familial	micropenis crytorchidism

Abbreviations are as follows: MAF, minor-allele frequency in gnomAD; KS, congenital hypogonadotropic hypogonadism plus anosmia (Kallmann syndrome); N/A: no DNA available; M, male; F, female.

Overall, NDNF mutations are present in nearly 2% of the CHH cohort (4/240). When only KS probands are considered, the frequency increases to ~3% (4/140).

Truncating NDNF Mutations Result in Loss of Function *In Vitro*

To evaluate the functionality of NDNF mutants *in vitro*, we assessed COS7 cells that had been transiently transfected with WT and mutant tagged NDNF cDNA for ectopic NDNF protein synthesis and secretion. Western-blot analysis of WT-transfected COS7 cells showed that NDNF protein is detected in both the conditioned medium and in the cell extract (Figures 2A and 2B). A radiolabeled-antibody binding assay showed expression at the cell surface (Figure 2C), suggesting that NDNF has either a direct or an extracellular-matrix-mediated interaction with cell-surface proteins.

Among the PTVs, the Lys62* and Tyr128Thrfs*55 mutants were not detected in whole cell extract or conditioned medium, suggesting disrupted protein synthesis or rapid degradation. In contrast, the Trp469* mutant is expressed in both the cell extract and conditioned medium but exhibits a reduced expression at the cell surface (50%). The Thr201Ser mutant displays no overall expression alterations (Figures 2A–2C).

We further examined the effect of WT NDNF on PLCgamma/Ca^{2+} pathway activation after FGF8 stimulation. As previously shown, FGF8 stimulation of FGFR1-transfected COS7 cells elicits a dose-dependent activation of the NFAT-luciferase reporter (Figure 2D).[37] Notably, when WT NDNF is co-transfected, the FGF8-induced NFAT reporter activity is inhibited in a dose-dependent fashion (Figure 2D). This assay was then used for evaluating the functionality of the expressed NDNF mutants. Whereas WT NDNF suppressed FGF8 signaling by 30%, the Trp469* mutant had no effect on FGF8 signaling, consistent with loss of function (Figure 2E). The Thr201Ser mutant and the WT suppressed FGF8 signaling similarly. Taken together, these combined *in vitro* results validate the three truncated mutants as causing a loss of function.

z-ndnf Contributes to GnRH Neuron Migration in Zebrafish

Using a previously validated MO-based strategy,[29] we depleted *z-ndnf* in zebrafish embryos and observed no gross morphological defects. We therefore depleted *z-ndnf*

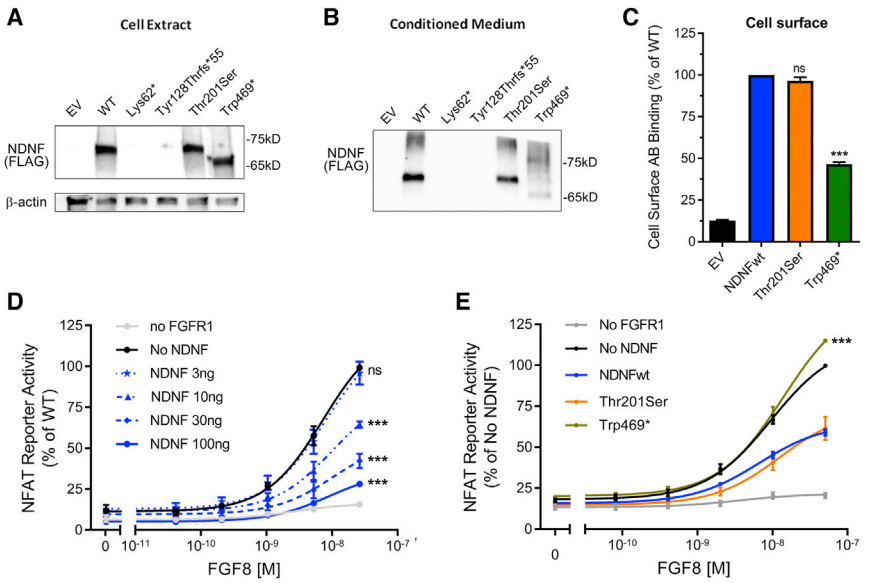

Figure 2. Truncated NDNF Variants Result in a Loss of Function *In Vitro*

(A and B) Representative experiments showing ectopic expression and secretion of NDNF protein. COS7 cells were transiently transfected with 5 or 100 ng of WT or mutant NDNF and analyzed by western blotting. The Lys62* and the Tyr128Thrfs*55 mutants were not detected. Thr201Ser and Trp469* were expressed at levels similar to those of the WT (means of five independent experiments).

(C) Cell-surface antibody binding of NDNF protein (means of four independent experiments). The expression of the truncated mutant Trp469* was decreased, whereas Thr201Ser was expressed at levels similar to those of the WT. ***$p < 0.001$; ns, not significant.

(D) NDNF suppresses FGF8 signaling in a dose-dependent manner. COS7 cells were transiently co-transfected with NFAT-luciferase reporter, FGFR1, and increasing doses of WT NDNF and treated with FGF8. ***$p < 0.001$; ns, not significant.

(E) Trp469* fails to inhibit FGF8 signaling. COS7 cells were transfected as described with 10 ng of WT or mutant NDNF. ***$p < 0.001$; ns, not significant.

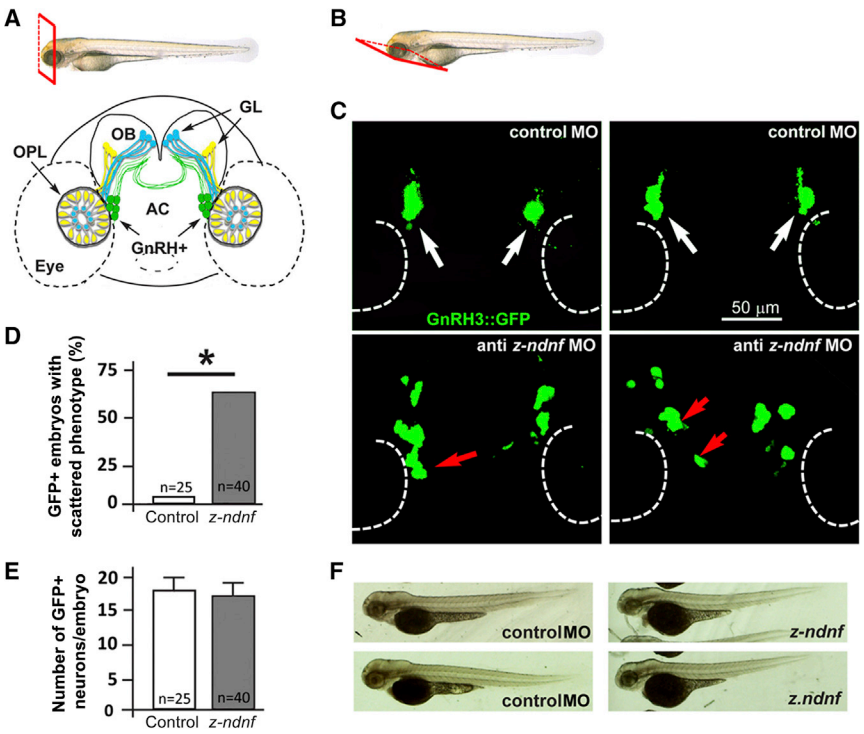

Figure 3. Depletion of *z-ndnf* in Zebrafish Resulted in Altered GnRH Neuron Position

(A) Schematic depiction showing the frontal view position of GnRH3::GFP+ neurons (green) relative to the olfactory placode (OPL), the olfactory bulb (OB), and the olfactory nerves (yellow and blue). The anterior commissure (AC) is shown at the base of the OB, GL, and glomeruli.

(B) Schematic depiction illustrating the ventral view used for fluorescence imaging.

(C) Micrographs of *GnRH3:GFP* zebrafish embryos at 72 hpf. The upper panels depict embryos injected with a control MO showing no significant alteration (white arrows), and the lower panels show embryos injected with anti-*z-ndnf* MO. The red arrows indicate mis-positioned GFP+ neurons.

(D) Percentage of embryos with "scattered GnRH neuron" phenotype in control versus anti-*z-ndnf* MOs, $p < 0.05$.

(E) Number of GFP+ neurons per embryo; there is no significant difference between the two groups.

(F) Whole-mount bright-field micrographs of control and injected embryos; The image shows normal embryonic morphology and size at 72 hpf.

in *GnRH3::GFP* transgenic embryos to specifically examine the number, position, and morphology of GnRH3-GFP$^+$ neurons. Injection of anti-*z-ndnf* MO did not affect GnRH3-GFP+ cell number (average 16 ± 1 per embryo at 72 hpf) or GFP fluorescence intensity (used here as a reporter of GnRH3 promoter). However, it did affect GnRH3-GFP+ neuron positioning along the known migratory route of the terminal nerve (Figure 3). Indeed, GnRH3-GFP+ neurons in embryos treated with control MO form a discrete aggregate between the olfactory placodes and the olfactory bulbs. In contrast, the *z-ndnf* embryos frequently exhibit severely mis-positioned or scattered GnRH3-GFP+ neurons (i.e., > 2 mis-positioned neurons in one half-embryo; 22/40 embryos [54%] in z-NDNF-MO versus 1/25 embryos in controls [4%]), consistent with a specific role of NDNF in the migration of GnRH neurons.

NDNF Is Expressed along the Migratory Route of Embryonic GnRH Cells in Mice and Humans

To determine whether *Ndnf* is expressed along the GnRH migratory pathway during mammalian embryonic development, we used a *GnRH::GFP* mouse model combined with FACS and qRT-PCR (Figures 4A and 4B). At E14.5, GnRH neurons are distributed throughout their migratory route, with approximately half in the nose and half in the brain (Figure 4A). *Ndnf* mRNA expression was very low in GnRH-GFP migratory cells in the nose, whereas *Ndnf* was strongly expressed by GFP-negative cells (e.g., olfactory and vomeronasal neurons, mesenchymal cells, and endothelial cells; Figure 4B). In the basal forebrain, *Ndnf* levels were low in both GnRH neurons and GFP-negative cells, suggesting that the major source of *Ndnf* at this stage is the nasal compartment. At E18.5, the GnRH migratory process is largely complete, and the majority of GnRH neurons have reached their target location in the hypothalamus. At this time point, *Ndnf* expression was significantly higher in GFP-negative cells than in GnRH neurons (Figure 4B).

Using double-immunofluorescence, we next evaluated the expression pattern of NDNF in the nasal compartment of human fetuses (7 and 11 GW) together with the expression of GnRH and TUJ1, a marker of the developing olfactory and vomeronasal systems and differentiated neurons (Figures 4C and 4D). NDNF was found in the developing olfactory epithelium, in the vomeronasal organ (VNO), and along the vomeronasal/terminal nerve (Figures 4C and 4D). At 7 GW, GnRH neurons were observed leaving the vomeronasal organ in close morphological association to NDNF-immunoreactive axons (Figure 4C). However, NDNF expression was absent from human migratory GnRH neurons.

NDNF Repels Migrating GnRH Cells *in vitro*

Since NDNF is highly expressed by olfactory and vomeronasal epithelia when GnRH neurons emerge from the VNO, we hypothesized that this soluble molecule could trigger GnRH directional migration by repelling these neurons from their site of origin and differentiation toward the forebrain (fb). We used GN11 cells, an *in vitro* model of migratory GnRH cells,[38] in a transwell plate assay to evaluate the response to increasing doses of recombinant human NDNF (10, 100, 200, 500 ng/mL). We added NDNF to either the upper chamber alone or the upper and lower

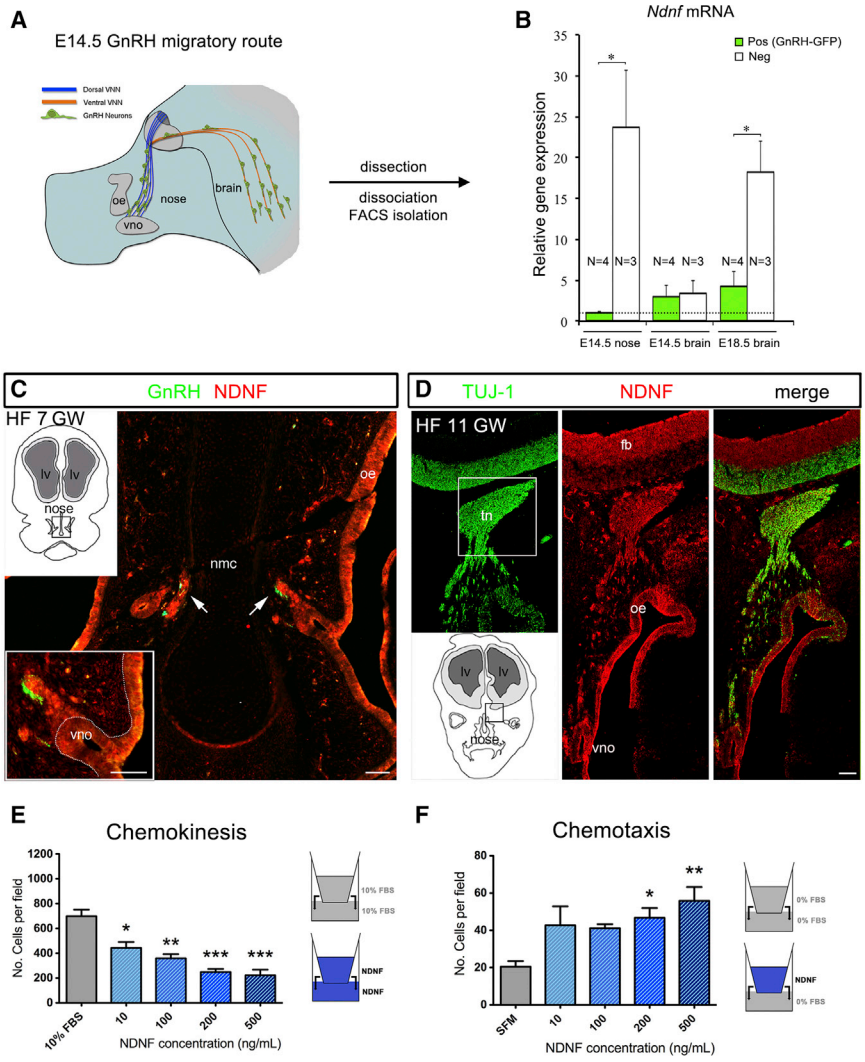

Figure 4. NDNF Expression Delineates the Migratory Route of Embryonic GnRH Cells in Mice and Humans and Repels Immortalized GnRH Cell Migration

(A) Schematic depiction of the GnRH migratory pathway in E14.5 mouse embryos (sagittal view).

(B) GFP-positive GnRH neurons and GFP-negative cells were isolated by FACS from the nasal region of E14.5 embryos (n = 3 or 4) and from the developing preoptic area of E14.5 (n = 3 or 4) and E18.5 (n = 3 or 4). Real-time PCR analysis helped to determine the expression levels of *Ndnf* mRNA in GFP-positive and -negative cells. Values are expressed relative to values, set at 1, in GnRH neurons at E14.5 and are shown as means ± SEM. One-way ANOVA followed by Tukey's Honest Significant Difference post-hoc analysis was used for comparing groups. *$p < 0.05$.

(C) Representative coronal section of a human fetus (HF) at 7 gestational weeks. The section is immunolabeled for GnRH and NDNF (n = 3). nmc, nasal midline cartilage; vno, vomeronasal organ.

(D) Representative coronal section of a human fetus at 11 gestational weeks. The section is immunolabeled for TUJ1 and NDNF (n = 3). tn, terminal nerve; fb, forebrain; oe, olfactory epithelium.

(E) For migration analysis, GN11 cells were used in a transwell assay in the presence or absence of recombinant NDNF (blue, both chambers).

(F) GN11 migration with NDNF in the upper chamber only (n = 5 for each treatment condition); *: $p < 0.05$, **: $p < 0.01$, ***: $p < 0.001$, one-way ANOVA followed by Tukey's post-hoc test. Scale bars in (C) represent 30 μm; scale bars in (D) represent 100 μm.

compartments of a transwell plate (Figures 4E and 4F) to specifically evaluate whether NDNF affects GN11 motility. This action can be through either chemokinesis or directional chemotaxis.

Exposure to increasing doses of NDNF plated in both chambers resulted in a significant reduction of GN11 cell migration to the bottom of the polycarbonate filter in comparison to what occurred in control conditions. This could be due to either an inhibition of cell motility or a repellent NDNF activity that neutralizes oriented migration when NDNF is present in both chambers. To investigate this further, we performed transwell migration assays by plating the same doses of NDNF in only the upper chamber in serum-free conditions (SFM). NDNF produced a significant increase in migration as compared to that in control conditions (Figure 4F). In combination with the expression data, these results suggest that NDNF acts as a chemorepellent molecule on GnRH cell migration.

To assess the functional consequences of NDNF mutants on GN11 directional migration, we performed three-dimensional matrix assays by co-culturing aggregates of GN11 cells for 72 h with aggregates of COS7 cells transiently transfected with a mock construct or with WT or mutant NDNF (Figure 5). Compared to the mock treatment, the WT NDNF GN11 cells displayed an asymmetrical distribution, with fewer cells on the proximal side and more cells on the distal side (Figure 5B). This asymmetrical migration confirmed the chemo-repulsive action of NDNF on immortalized GnRH neurons. However, this directional effect was prevented when GN11 cells were co-cultured with COS7 cells expressing any of the NDNF mutants. These results show that WT NDNF acts as a chemorepellent for GnRH cell migration and that this effect is lost in NDNF mutants, including the Thr201Ser mutant.

Loss of *Ndnf* in Murine Embryos Alters GnRH Neuron Migration and the Olfactory Axonal Scaffold

We then sought to determine whether genetic deletion of *Ndnf* in a murine model would lead to defects in GnRH neuronal migration. We performed a detailed analysis of E13.5 *Ndnf* WT, heterozygous, and homozygous mutants by using whole-mount immunostaining for

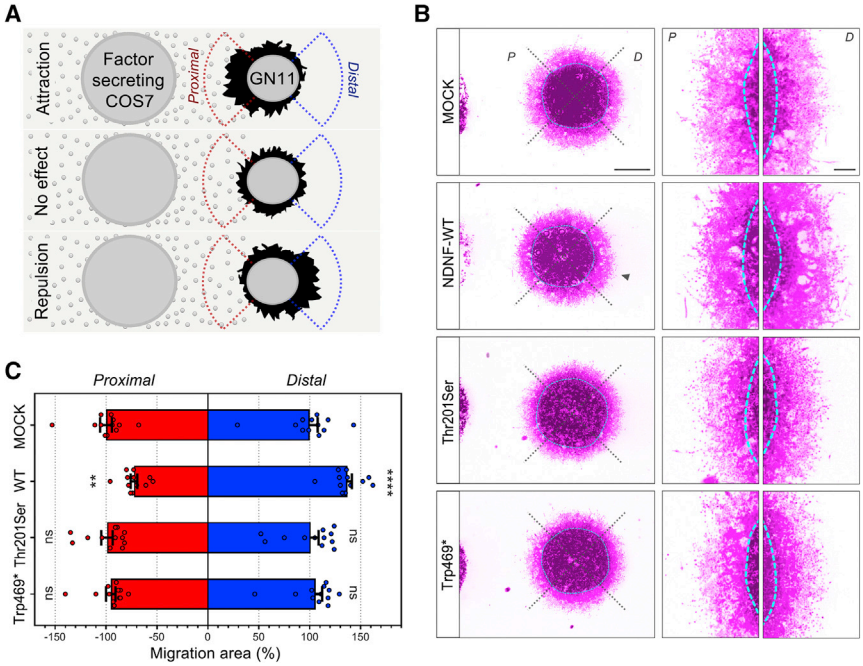

Figure 5. NDNF Mutants Fail to Induce GnRH Cell Migration *In Vitro*

(A) Schematic illustration of the three-dimensional co-cultures of COS7 and GN11 cell aggregates. After 72 h in culture, the GN11 migration area is measured in the proximal (red) and distal (blue) quadrants as the surface covered by GN11 cells minus the aggregate inner mass area.

(B) Representative pictures of three-dimensional matrix co-cultures of GN11 cells with COS7 cells stained withDAPI and phalloidin red. For illustration, photographs have been digitally inverted, and a pseudo-color (purple) has been superimposed so that cell distribution is highlighted.

(C) Quantitative analysis of GN11 cell-migration aggregates (n = 12 per group) normalized and compared to the control condition (MOCK). Values are expressed as means ± SEM and analyzed by two-way ANOVA followed by Sidak's multiple-comparisons test. **p < 0.01; ****p < 0.0001. d, distal side; p, proximal side.

GnRH and peripherin, a neuron-specific intermediate filament protein expressed by rodent sensory and autonomic axons,[39] including the developing olfactory nerve (ON) and the vomeronasal nerve (VNN).[35,40] This was followed by iDISCO tissue clearing[36] and light-sheet microscopy (LSM) (Figures 6A–6D; Videos S1 and S2). In *Ndnf*$^{+/+}$ embryos, GnRH neurons were more clustered in the nasal compartment, and fewer GnRH cells reached the developing hypothalamus at this embryonic stage (Figures 6A–6D, arrowheads; Videos S1 and S2). Moreover, in *Ndnf*$^{+/+}$ embryos, peripherin-positive fibers were seen to almost completely innervate the olfactory bulb (Figures 6E and 6G, arrows), whereas in *Ndnf*$^{-/-}$ mice olfactory axons only partially innervate their target tissues (Figures 6F and 6H, arrows). The intracranial projections of the terminal and vomeronasal nerve (tn/vnn) did not show any abnormalities in *Ndnf*$^{-/-}$embryos as compared to *Ndnf*$^{+/+}$ embryos (Figures 6E and 6F).

We then counted the number of GnRH neurons in these embryos and found a comparable total number of GnRH neurons between all genotypes (Figure 6I), indicating that a lack of *Ndnf* has no effect on GnRH neuron survival. However, in *Ndnf*$^{-/-}$ mice the number of GnRH cells in the nasal and olfactory bulb region was significantly greater than in *Ndnf*$^{+/+}$or *Ndnf*$^{+/-}$mice (Figure 6J), respectively. As a result, fewer GnRH neurons reached the hypothalamic region in the *Ndnf*-null embryos (Figure 6J). The accumulation of GnRH neurons in the more rostral regions and decreased cell number within the ventral forebrain is suggestive of a delayed GnRH cell migration in *Ndnf*$^{-/-}$ mice.

Altogether, these experiments revealed that genetic invalidation of *Ndnf* leads to abnormal development of the olfactory system and defective GnRH migration to the hypothalamus.

Discussion

NDNF, the neuron-derived neurotrophic factor, was identified as a CHH gene via a strategy including WES and bioinformatics and focusing on genes in the FN3 superfamily. We first identified an enrichment of *NDNF* PTVs in our CHH cohort versus gnomAD. The three unrelated CHH probands (~2%) harboring heterozygous protein-truncating *NDNF* mutations had severe GnRH deficiency and anosmia consistent with Kallmann syndrome. Because *Ndnf* had been previously implicated in neuron structural plasticity, we then silenced *z-ndnf* in zebrafish, which resulted in a defect in GnRH neuron migration. *In vitro* studies established NDNF as a chemorepellent factor; combined with this protein's high expression in the nasal compartment, this finding could indicate a role for NDNF in initiating GnRH neuron migration.

CHH is a complex genetic disorder for which >40 associated loci, each accounting for less than 10% of cases, have been identified to date. Importantly, about half of persons with CHH do not carry mutations in the known CHH-associated genes.[3] Historically, cytogenetics,[41–45] linkage studies,[46,47] homozygosity mapping,[48] candidate gene approaches,[1,49] and other strategies have been used for the discovery of new genes related to CHH. Recently, Guo et al. applied collapsed gene-based burden testing to a population of 393 unrelated CHH probands and demonstrated significant associations to only three of the known CHH-related genes—*FGFR1* [MIM: 136350], *TACR3* [MIM: 162332], and *GNRHR* [MIM: 138850].[16] Limitations of the study included a small population size and an inability to detect significant associations to most of the known CHH-related genes. Our current strategy combined collapsed gene-based burden

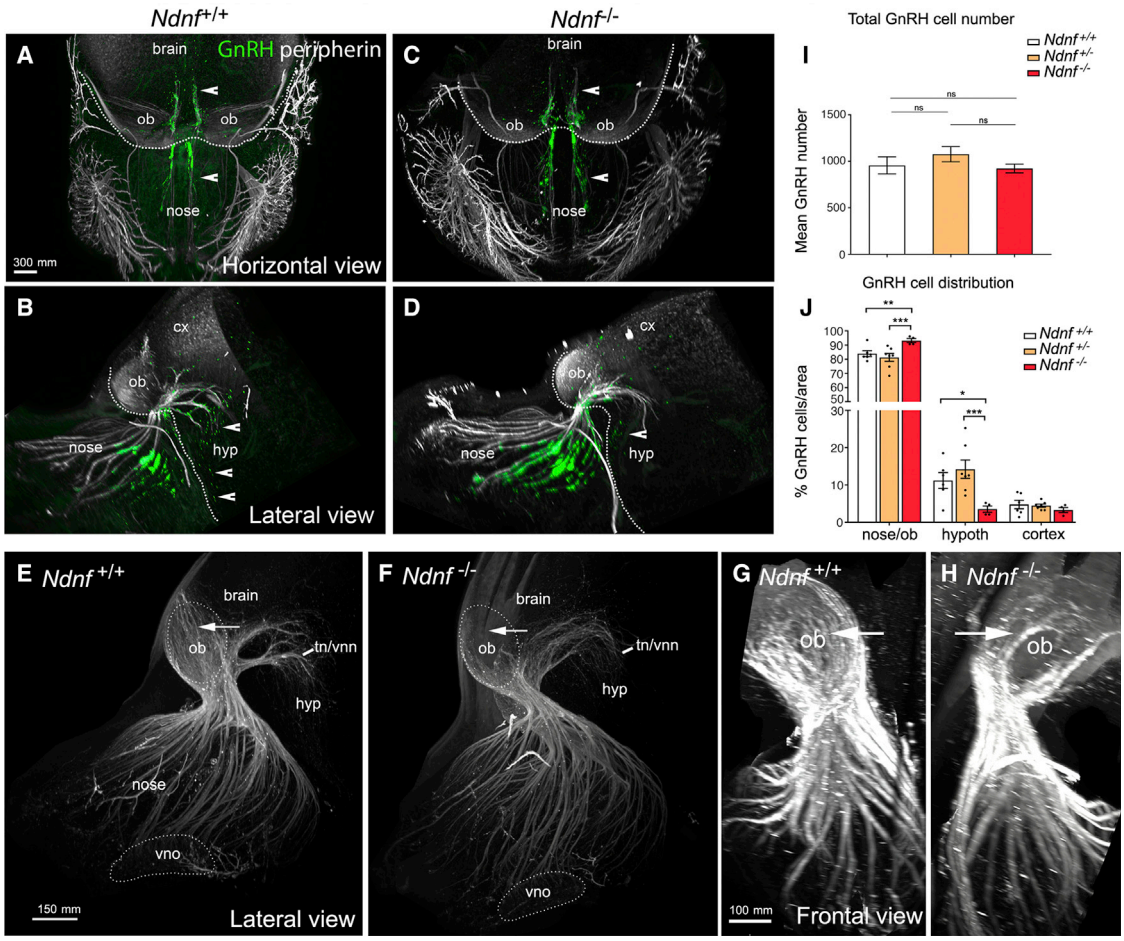

Figure 6. GnRH Migration and Olfactory Innervation Are Perturbed in *Ndnf*$^{-/-}$ Mice

(A–D) Representative whole-body iDISCO experiments in E13.5 *Ndnf*$^{+/+}$and *Ndnf*$^{-/-}$embryos immunolabelled for peripherin (white) and GnRH (green). (A and C) Horizontal projections of the embryo heads. (B and D) Lateral projections of the embryo heads. Arrowheads in A–D indicate GnRH cells located in the nasal and brain regions.

(E and F) High-magnification photomicrographs (lateral view) depicting olfactory and vomeronasal axon innervations (peripherin-positive) to the olfactory bulb and to the presumptive hypothalamus (terminal and vomeronasal nerve, tn/vnn) in E13.5 *Ndnf*$^{+/+}$(E) and *Ndnf*$^{-/-}$embryos (F).

(G and H) High-power view (frontal view) showing olfactory axon innervations of the OB in E13.5 *Ndnf*$^{+/+}$(G) and *Ndnf*$^{-/-}$ (H) embryos. Arrows in (E)–(H) indicate noticeable differences in peripherin-positive fibers innervating the OB.

(I) Quantification of the total number of GnRH-immunoreactive neurons in *Ndnf*$^{+/+}$(n = 6), *Ndnf*$^{+/-}$(n = 7), and *Ndnf*$^{-/-}$ E13.5 embryos (n = 4). Data are represented as means ± SEM. Statistical analysis was performed by one-way ANOVA ($F_{2,14} = 0.9$, p = 0.4) followed by Fisher's LSD post-hoc test.

(J) Quantitative analysis of GnRH neuronal distribution throughout the migratory pathway in the three experimental populations. Statistical analysis was performed by two-way ANOVA ($F_{4,42} = 7.58$, p = 0.0001) followed by Fisher's LSD post-hoc test (*p < 0.05, **p < 0.005, ***p < 0.001). Scale bars (A–D) represent 200 μm.

testing with a targeted gene population (FN3 superfamily). This approach was based on the observation that several proteins that were involved in GnRH neuron migration and that were previously implicated in CHH (e.g., such proteins include ANOS1, AXL, DCC, and FLRT3*)* contain FN3 domains. Through the study of 240 CHH-unrelated probands, we demonstrated a statistical enrichment for PTVs in *NDNF*, which encodes a secreted glycosylated disulfide-bond protein containing FN3 domains. In addition, two known FN3-containing CHH-related genes (*ANOS1* and *AXL*) also gave positive associations.[16]

The enrichment of PTVs in *NDNF* suggests that deletions in *NDNF* might explain some cases of CHH and will be further studied via whole-genome sequencing. Indeed, pathogenic deletions have been reported for other genes underlying CHH (e.g., such genes include *ANOS1*,[50] *SEMA3A*,[51] *PROKR2*,[52] *FGFR1*,[53] and, *SOX10*[54]*).*

The four probands carrying a heterozygous *NDNF* mutation exhibited both CHH and anosmia (i.e., KS), a condition related to defects in the embryonic development of GnRH neurons.[1] Overall, ~3% of individuals with KS harbor *NDNF* mutations. Notably, several family members carrying *NDNF* mutations also exhibit a partial phenotype (i.e., delay of puberty and/or anosmia), consistent with an autosomal-dominant mode of inheritance with variable expressivity and incomplete penetrance—features seen in

other CHH-related genes.[1,2] None of the probands harbor mutations in other known CHH-related genes.[1,2,55] As new research disentangles the NDNF signaling pathway (including its receptor), novel genetic interactions might be uncovered. Further investigations are needed to dissect the contribution of genetic (e.g., oligogenicity, structural variants, and eQTLs) and environmental factors (e.g., stress, nutrition, and endocrine disruptors) potentially modifying the phenotype of persons carrying *NDNF* loss-of-function mutations.

NDNF is a secreted neurotrophic factor that can promote neuron migration, growth, and survival, as well as neurite outgrowth.[11] *Ndnf* is highly expressed in the olfactory bulb, Cajal-Retzius cells, hippocampus, and cerebellum during murine embryogenesis.[11] Herein, we show that NDNF is expressed in the nasal region after formation of the olfactory placode in mice and humans, although not in GnRH neurons. Furthermore, the NDNF spatio-temporal expression pattern overlaps the GnRH neuron migratory route. In addition to the NDNF expression pattern, the positive effect of recombinant NDNF on GnRH neuron migration *in vitro* and the migratory defect of GnRH neurons in both z-*ndnf* MO-injected zebrafish and *Ndnf*-null mice provides strong evidence for a role of NDNF in GnRH neuron migration.

There are similarities between the two extracellular matrix proteins NDNF and anosmin-1, which is encoded by the first KS-related gene discovered, *ANOS1*. Indeed, both contain FN3 domains that are critical for binding to heparan sulfate proteoglycans.[11,51] Anosmin-1 modulates FGFR1 signaling via a direct interaction of the anosmin-1-FN3 domain with heparan sulfate proteoglycan.[56] Our *in vitro* studies demonstrate that NDNF also modulates FGFR1 signaling by inhibiting FGFR1-induced PLCγ/Ca^{2+} pathway activation after FGF8 stimulation. Thus, NDNF could interact *in vivo* with FGF8, a well-known morphogen acting during early developmental stages on the fate specification of GnRH neurons in the olfactory placode. Further studies investigating this process *in vivo* are needed.

Finally, NDNF promotes endothelial cell survival and vessel formation and, thus, is a powerful angiogenic factor.[57,58] NDNF modulates endothelial plasticity through AKT/eNOS signaling,[58] which is also known to be crucial for GnRH release in the median eminence.[59–61] This suggests a possible role of NDNF in GnRH neuron biology beyond embryonic development.

In conclusion, we have identified *NDNF* as a novel factor involved in GnRH neuron ontogeny in humans and mice. Identifying the molecular signaling pathway used by NDNF in GnRH neuron ontogeny, along with the which particular receptors and upstream and downstream targets are involved, will be critical. Furthermore, it will also be crucial to study the role of NDNF in the adult GnRH system and homeostasis, specifically in regard to pubertal onset and fertility.

Supplemental Data

Supplemental Data can be found online at https://doi.org/10.1016/j.ajhg.2019.12.003.

Acknowledgments

We are grateful to the affected individuals and their families for their invaluable participation in this study, as well as to Erik Hrabovszky (Institute of Experimental Medicine, University of Budapest, Hungary) and Daniel J. Spergel (Section of Endocrinology, Department of Medicine, University of Chicago, IL) for providing anti-GnRH antibodies and *GnRH-GFP* mice, respectively. We also acknowledge Harri Niinikoski from the University of Turku for referring a CHH proband with an *NDNF* mutation, Kirsi Sainio from University of Helsinki for her guidance on mouse embryo harvesting, as well as M. Tardivel and A. Bongiovanni (microscopy core facility of Bioimaging Center Lille [BICeL], Lille University School of Medicine) for their technical assistance. We thank our colleagues Lucia Bartoloni, Alexia Spoerl, and Jenny Meylan of the Diagnostic Laboratory of Endocrine Genetic Diseases of the CHUV for their precious assistance in DNA sample preparation. This work was supported by Swiss National Foundation (N.P.) grant 310030_173260, the Institut National de la Santé et de la Recherche Médicale, Inserm, France (grant number U1172), the Agence Nationale de la Recherche, France (grant numbers ANR-14-CE12-0015-01 and ANR-18-CE14-0017-02 to P.G.), and Fondazione CRT (Torino, ITALY # 2014-0814 to G.R.M).

Declaration of Interests

The authors declare no competing interests.

Received: July 22, 2019
Accepted: November 22, 2019
Published: December 26, 2019

Web Resources

GnomAD, https://gnomad.broadinstitute.org/
Interpro, https://www.ebi.ac.uk/interpro
HGNC, https://www.genenames.org/
OMIM, http://www.omim.org/.

References

1. Boehm, U., Bouloux, P.M., Dattani, M.T., de Roux, N., Dodé, C., Dunkel, L., Dwyer, A.A., Giacobini, P., Hardelin, J.P., Juul, A., et al. (2015). Expert consensus document: European Consensus Statement on congenital hypogonadotropic hypogonadism–pathogenesis, diagnosis and treatment. Nat. Rev. Endocrinol. *11*, 547–564.
2. Young, J., Xu, C., Papadakis, G.E., Acierno, J.S., Maione, L., Hietamäki, J., Raivio, T., and Pitteloud, N. (2019). Clinical management of congenital hypogonadotropic hypogonadism. Endocr. Rev. *40*, 669–710.
3. Cassatella, D., Howard, S.R., Acierno, J.S., Xu, C., Papadakis, G.E., Santoni, F.A., Dwyer, A.A., Santini, S., Sykiotis, G.P., Chambion, C., et al. (2018). Congenital hypogonadotropic hypogonadism and constitutional delay of growth and puberty have distinct genetic architectures. European J. Endocrinol. *178*, 377–388.

4. Schwanzel-Fukuda, M., and Pfaff, D.W. (1989). Origin of luteinizing hormone-releasing hormone neurons. Nature *338*, 161–164.
5. Wray, S. (2010). From nose to brain: development of gonadotrophin-releasing hormone-1 neurones. J. Neuroendocrinol. *22*, 743–753.
6. Wierman, M.E., Kiseljak-Vassiliades, K., and Tobet, S. (2011). Gonadotropin-releasing hormone (GnRH) neuron migration: initiation, maintenance and cessation as critical steps to ensure normal reproductive function. Front. Neuroendocrinol. *32*, 43–52.
7. Schwanzel-Fukuda, M., Bick, D., and Pfaff, D.W. (1989). Luteinizing hormone-releasing hormone (LHRH)-expressing cells do not migrate normally in an inherited hypogonadal (Kallmann) syndrome. Brain Res. Mol. Brain Res. *6*, 311–326.
8. del Castillo, I., Cohen-Salmon, M., Blanchard, S., Lutfalla, G., and Petit, C. (1992). Structure of the X-linked Kallmann syndrome gene and its homologous pseudogene on the Y chromosome. Nat. Genet. *2*, 305–310.
9. Bork, P., and Doolittle, R.F. (1992). Proposed acquisition of an animal protein domain by bacteria. Proc. Natl. Acad. Sci. USA *89*, 8990–8994.
10. Bencharit, S., Cui, C.B., Siddiqui, A., Howard-Williams, E.L., Sondek, J., Zuobi-Hasona, K., and Aukhil, I. (2007). Structural insights into fibronectin type III domain-mediated signaling. J. Mol. Biol. *367*, 303–309.
11. Kuang, X.L., Zhao, X.M., Xu, H.F., Shi, Y.Y., Deng, J.B., and Sun, G.T. (2010). Spatio-temporal expression of a novel neuron-derived neurotrophic factor (NDNF) in mouse brains during development. BMC Neurosci. *11*, 137.
12. Oliveira, L.M., Seminara, S.B., Beranova, M., Hayes, F.J., Valkenburgh, S.B., Schipani, E., Costa, E.M., Latronico, A.C., Crowley, W.F., Jr., and Vallejo, M. (2001). The importance of autosomal genes in Kallmann syndrome: genotype-phenotype correlations and neuroendocrine characteristics. J. Clin. Endocrinol. Metab. *86*, 1532–1538.
13. Seminara, S.B., Oliveira, L.M., Beranova, M., Hayes, F.J., and Crowley, W.F., Jr. (2000). Genetics of hypogonadotropic hypogonadism. J. Endocrinol. Invest. *23*, 560–565.
14. Xu, C., Messina, A., Somm, E., Miraoui, H., Kinnunen, T., Acierno, J., Jr., Niederländer, N.J., Bouilly, J., Dwyer, A.A., Sidis, Y., et al. (2017). *KLB*, encoding β-Klotho, is mutated in patients with congenital hypogonadotropic hypogonadism. EMBO Mol. Med. *9*, 1379–1397.
15. Laitinen, E.M., Vaaralahti, K., Tommiska, J., Eklund, E., Tervaniemi, M., Valanne, L., and Raivio, T. (2011). Incidence, phenotypic features and molecular genetics of Kallmann syndrome in Finland. Orphanet J. Rare Dis. *6*, 41.
16. Guo, M.H., Plummer, L., Chan, Y.M., Hirschhorn, J.N., and Lippincott, M.F. (2018). Burden testing of rare variants identified through exome sequencing via publicly available control data. Am. J. Hum. Genet. *103*, 522–534.
17. Raivio, T., Sidis, Y., Plummer, L., Chen, H., Ma, J., Mukherjee, A., Jacobson-Dickman, E., Quinton, R., Van Vliet, G., Lavoie, H., et al. (2009). Impaired fibroblast growth factor receptor 1 signaling as a cause of normosmic idiopathic hypogonadotropic hypogonadism. J. Clin. Endocrinol. Metab. *94*, 4380–4390.
18. Ichida, M., and Finkel, T. (2001). Ras regulates NFAT3 activity in cardiac myocytes. J. Biol. Chem. *276*, 3524–3530.
19. Crabtree, G.R., and Olson, E.N. (2002). NFAT signaling: choreographing the social lives of cells. Cell *109*, S67–S79.
20. Messina, A., Ferraris, N., Wray, S., Cagnoni, G., Donohue, D.E., Casoni, F., Kramer, P.R., Derijck, A.A., Adolfs, Y., Fasolo, A., et al. (2011). Dysregulation of Semaphorin7A/β1-integrin signaling leads to defective GnRH-1 cell migration, abnormal gonadal development and altered fertility. Hum. Mol. Genet. *20*, 4759–4774.
21. Giacobini, P., Messina, A., Morello, F., Ferraris, N., Corso, S., Penachioni, J., Giordano, S., Tamagnone, L., and Fasolo, A. (2008). Semaphorin 4D regulates gonadotropin hormone-releasing hormone-1 neuronal migration through PlexinB1-Met complex. J. Cell Biol. *183*, 555–566.
22. Yoshida, T., Ito, A., Matsuda, N., and Mishina, M. (2002). Regulation by protein kinase A switching of axonal pathfinding of zebrafish olfactory sensory neurons through the olfactory placode-olfactory bulb boundary. J. Neurosci. *22*, 4964–4972.
23. Miyasaka, N., Sato, Y., Yeo, S.Y., Hutson, L.D., Chien, C.B., Okamoto, H., and Yoshihara, Y. (2005). Robo2 is required for establishment of a precise glomerular map in the zebrafish olfactory system. Development *132*, 1283–1293.
24. Sato, Y., Miyasaka, N., and Yoshihara, Y. (2005). Mutually exclusive glomerular innervation by two distinct types of olfactory sensory neurons revealed in transgenic zebrafish. J. Neurosci. *25*, 4889–4897.
25. Garaffo, G., Conte, D., Provero, P., Tomaiuolo, D., Luo, Z., Pinciroli, P., Peano, C., D'Atri, I., Gitton, Y., Etzion, T., et al. (2015). The Dlx5 and Foxg1 transcription factors, linked via miRNA-9 and -200, are required for the development of the olfactory and GnRH system. Mol. Cell. Neurosci. *68*, 103–119.
26. Abraham, E., Palevitch, O., Gothilf, Y., and Zohar, Y. (2010). Targeted gonadotropin-releasing hormone-3 neuron ablation in zebrafish: effects on neurogenesis, neuronal migration, and reproduction. Endocrinology *151*, 332–340.
27. Flynt, A.S., Li, N., Thatcher, E.J., Solnica-Krezel, L., and Patton, J.G. (2007). Zebrafish miR-214 modulates Hedgehog signaling to specify muscle cell fate. Nat. Genet. *39*, 259–263.
28. Kloosterman, W.P., and Plasterk, R.H. (2006). The diverse functions of microRNAs in animal development and disease. Dev. Cell *11*, 441–450.
29. Melvin, V.S., Feng, W., Hernandez-Lagunas, L., Artinger, K.B., and Williams, T. (2013). A morpholino-based screen to identify novel genes involved in craniofacial morphogenesis. Dev. Dyn. *242*, 817–831.
30. Garaffo, G., Provero, P., Molineris, I., Pinciroli, P., Peano, C., Battaglia, C., Tomaiuolo, D., Etzion, T., Gothilf, Y., Santoro, M., and Merlo, G.R. (2013). Profiling, bioinformatic, and functional data on the developing olfactory/GnRH system reveal cellular and molecular pathways essential for this process and potentially relevant for the Kallmann Syndrome. Front. Endocrinol. (Lausanne) *4*, 203.
31. Tang, R., Dodd, A., Lai, D., McNabb, W.C., and Love, D.R. (2007). Validation of zebrafish (Danio rerio) reference genes for quantitative real-time RT-PCR normalization. Acta Biochim. Biophys. Sin. (Shanghai) *39*, 384–390.
32. Spergel, D.J., Krüth, U., Hanley, D.F., Sprengel, R., and Seeburg, P.H. (1999). GABA- and glutamate-activated channels in green fluorescent protein-tagged gonadotropin-releasing hormone neurons in transgenic mice. J. Neurosci. *19*, 2037–2050.
33. Parkash, J., Cimino, I., Ferraris, N., Casoni, F., Wray, S., Cappy, H., Prevot, V., and Giacobini, P. (2012). Suppression of β1-integrin in gonadotropin-releasing hormone cells disrupts

migration and axonal extension resulting in severe reproductive alterations. J. Neurosci. *32*, 16992–17002.
34. Giacobini, P., Parkash, J., Campagne, C., Messina, A., Casoni, F., Vanacker, C., Langlet, F., Hobo, B., Cagnoni, G., Gallet, S., et al. (2014). Brain endothelial cells control fertility through ovarian-steroid-dependent release of semaphorin 3A. PLoS Biol. *12*, e1001808.
35. Casoni, F., Malone, S.A., Belle, M., Luzzati, F., Collier, F., Allet, C., Hrabovszky, E., Rasika, S., Prevot, V., Chédotal, A., and Giacobini, P. (2016). Development of the neurons controlling fertility in humans: new insights from 3D imaging and transparent fetal brains. Development *143*, 3969–3981.
36. Renier, N., Wu, Z., Simon, D.J., Yang, J., Ariel, P., and Tessier-Lavigne, M. (2014). iDISCO: a simple, rapid method to immunolabel large tissue samples for volume imaging. Cell *159*, 896–910.
37. Goetz, R., and Mohammadi, M. (2013). Exploring mechanisms of FGF signalling through the lens of structural biology. Nat. Rev. Mol. Cell Biol. *14*, 166–180.
38. Radovick, S., Wray, S., Lee, E., Nicols, D.K., Nakayama, Y., Weintraub, B.D., Westphal, H., Cutler, G.B., Jr., and Wondisford, F.E. (1991). Migratory arrest of gonadotropin-releasing hormone neurons in transgenic mice. Proc. Natl. Acad. Sci. USA *88*, 3402–3406.
39. Parysek, L.M., and Goldman, R.D. (1988). Distribution of a novel 57 kDa intermediate filament (IF) protein in the nervous system. J. Neurosci. *8*, 555–563.
40. Fueshko, S., and Wray, S. (1994). LHRH cells migrate on peripherin fibers in embryonic olfactory explant cultures: an in vitro model for neurophilic neuronal migration. Dev. Biol. *166*, 331–348.
41. Meitinger, T., Heye, B., Petit, C., Levilliers, J., Golla, A., Moraine, C., Dalla Piccola, B., Sippell, W.G., Murken, J., and Ballabio, A. (1990). Definitive localization of X-linked Kallman syndrome (hypogonadotropic hypogonadism and anosmia) to Xp22.3: close linkage to the hypervariable repeat sequence CRI-S232. Am. J. Hum. Genet. *47*, 664–669.
42. Legouis, R., Hardelin, J.P., Levilliers, J., Claverie, J.M., Compain, S., Wunderle, V., Millasseau, P., Le Paslier, D., Cohen, D., Caterina, D., et al. (1991). The candidate gene for the X-linked Kallmann syndrome encodes a protein related to adhesion molecules. Cell *67*, 423–435.
43. Dodé, C., Levilliers, J., Dupont, J.M., De Paepe, A., Le Dû, N., Soussi-Yanicostas, N., Coimbra, R.S., Delmaghani, S., Compain-Nouaille, S., Baverel, F., et al. (2003). Loss-of-function mutations in FGFR1 cause autosomal dominant Kallmann syndrome. Nat. Genet. *33*, 463–465.
44. de Roux, N., Young, J., Misrahi, M., Genet, R., Chanson, P., Schaison, G., and Milgrom, E. (1997). A family with hypogonadotropic hypogonadism and mutations in the gonadotropin-releasing hormone receptor. N. Engl. J. Med. *337*, 1597–1602.
45. Franco, B., Guioli, S., Pragliola, A., Incerti, B., Bardoni, B., Tonlorenzi, R., Carrozzo, R., Maestrini, E., Pieretti, M., Taillon-Miller, P., et al. (1991). A gene deleted in Kallmann's syndrome shares homology with neural cell adhesion and axonal pathfinding molecules. Nature *353*, 529–536.
46. de Roux, N., Genin, E., Carel, J.C., Matsuda, F., Chaussain, J.L., and Milgrom, E. (2003). Hypogonadotropic hypogonadism due to loss of function of the KiSS1-derived peptide receptor GPR54. Proc. Natl. Acad. Sci. USA *100*, 10972–10976.
47. Seminara, S.B., Messager, S., Chatzidaki, E.E., Thresher, R.R., Acierno, J.S., Jr., Shagoury, J.K., Bo-Abbas, Y., Kuohung, W., Schwinof, K.M., Hendrick, A.G., et al. (2003). The GPR54 gene as a regulator of puberty. N. Engl. J. Med. *349*, 1614–1627.
48. Topaloglu, A.K., Reimann, F., Guclu, M., Yalin, A.S., Kotan, L.D., Porter, K.M., Serin, A., Mungan, N.O., Cook, J.R., Imamoglu, S., et al. (2009). TAC3 and TACR3 mutations in familial hypogonadotropic hypogonadism reveal a key role for Neurokinin B in the central control of reproduction. Nat. Genet. *41*, 354–358.
49. Stamou, M.I., Cox, K.H., and Crowley, W.F., Jr. (2016). Discovering genes essential to the hypothalamic regulation of human reproduction using a human disease model: Adjusting to life in the "-omics" era. Endocr. Rev. *2016*, 4–22.
50. Ballabio, A., Bardoni, B., Carrozzo, R., Andria, G., Bick, D., Campbell, L., Hamel, B., Ferguson-Smith, M.A., Gimelli, G., Fraccaro, M., et al. (1989). Contiguous gene syndromes due to deletions in the distal short arm of the human X chromosome. Proc. Natl. Acad. Sci. USA *86*, 10001–10005.
51. Young, J., Metay, C., Bouligand, J., Tou, B., Francou, B., Maione, L., Tosca, L., Sarfati, J., Brioude, F., Esteva, B., et al. (2012). SEMA3A deletion in a family with Kallmann syndrome validates the role of semaphorin 3A in human puberty and olfactory system development. Hum. Reprod. *27*, 1460–1465.
52. Pitteloud, N., Zhang, C., Pignatelli, D., Li, J.D., Raivio, T., Cole, L.W., Plummer, L., Jacobson-Dickman, E.E., Mellon, P.L., Zhou, Q.Y., and Crowley, W.F., Jr. (2007). Loss-of-function mutation in the prokineticin 2 gene causes Kallmann syndrome and normosmic idiopathic hypogonadotropic hypogonadism. Proc. Natl. Acad. Sci. USA *104*, 17447–17452.
53. Trarbach, E.B., Teles, M.G., Costa, E.M., Abreu, A.P., Garmes, H.M., Guerra, G., Jr., Baptista, M.T., de Castro, M., Mendonca, B.B., and Latronico, A.C. (2010). Screening of autosomal gene deletions in patients with hypogonadotropic hypogonadism using multiplex ligation-dependent probe amplification: detection of a hemizygosis for the fibroblast growth factor receptor 1. Clin. Endocrinol. (Oxf.) *72*, 371–376.
54. Amato, L.G.L., Montenegro, L.R., Lerario, A.M., Jorge, A.A.L., Guerra Junior, G., Schnoll, C., Renck, A.C., Trarbach, E.B., Costa, E.M.F., Mendonca, B.B., et al. (2019). New genetic findings in a large cohort of congenital hypogonadotropic hypogonadism. Eur. J. Endocrinol. *181*, 103–119.
55. Pitteloud, N., Quinton, R., Pearce, S., Raivio, T., Acierno, J., Dwyer, A., Plummer, L., Hughes, V., Seminara, S., Cheng, Y.Z., et al. (2007). Digenic mutations account for variable phenotypes in idiopathic hypogonadotropic hypogonadism. J. Clin. Invest. *117*, 457–463.
56. González-Martínez, D., Kim, S.H., Hu, Y., Guimond, S., Schofield, J., Winyard, P., Vannelli, G.B., Turnbull, J., and Bouloux, P.M. (2004). Anosmin-1 modulates fibroblast growth factor receptor 1 signaling in human gonadotropin-releasing hormone olfactory neuroblasts through a heparan sulfate-dependent mechanism. J. Neurosci. *24*, 10384–10392.
57. Ohashi, K., Enomoto, T., Joki, Y., Shibata, R., Ogura, Y., Kataoka, Y., Shimizu, Y., Kambara, T., Uemura, Y., Yuasa, D., et al. (2014). Neuron-derived neurotrophic factor functions as a novel modulator that enhances endothelial cell function and revascularization processes. J. Biol. Chem. *289*, 14132–14144.
58. Joki, Y., Ohashi, K., Yuasa, D., Shibata, R., Kataoka, Y., Kambara, T., Uemura, Y., Matsuo, K., Hayakawa, S., Hiramatsu-Ito, M., et al. (2015). Neuron-derived neurotrophic factor

ameliorates adverse cardiac remodeling after experimental myocardial infarction. Circ Heart Fail *8*, 342–351.

59. Aguan, K., Mahesh, V.B., Ping, L., Bhat, G., and Brann, D.W. (1996). Evidence for a physiological role for nitric oxide in the regulation of the LH surge: effect of central administration of antisense oligonucleotides to nitric oxide synthase. Neuroendocrinology *64*, 449–455.
60. De Seranno, S., Estrella, C., Loyens, A., Cornea, A., Ojeda, S.R., Beauvillain, J.C., and Prevot, V. (2004). Vascular endothelial cells promote acute plasticity in ependymoglial cells of the neuroendocrine brain. J. Neurosci. *24*, 10353–10363.
61. de Seranno, S., d'Anglemont de Tassigny, X., Estrella, C., Loyens, A., Kasparov, S., Leroy, D., Ojeda, S.R., Beauvillain, J.C., and Prevot, V. (2010). Role of estradiol in the dynamic control of tanycyte plasticity mediated by vascular endothelial cells in the median eminence. Endocrinology *151*, 1760–1772.

The American Journal of Human Genetics, Volume *106*

Supplemental Data

Neuron-Derived Neurotrophic Factor

Is Mutated in Congenital Hypogonadotropic Hypogonadism

Andrea Messina, Kristiina Pulli, Sara Santini, James Acierno, Johanna Känsäkoski, Daniele Cassatella, Cheng Xu, Filippo Casoni, Samuel A. Malone, Gaetan Ternier, Daniele Conte, Yisrael Sidis, Johanna Tommiska, Kirsi Vaaralahti, Andrew Dwyer, Yoav Gothilf, Giorgio R. Merlo, Federico Santoni, Nicolas J. Niederländer, Paolo Giacobini, Taneli Raivio, and Nelly Pitteloud

Cases Descriptions

Family #1: *NDNF* p.Lys62* (heterozygous)

The Caucasian male proband was born with cryptorchidism and micropenis. He presented at the age 17 years for failure to undergo spontaneous puberty. At that time, he had prepubertal testis (testicular volume <3 ml) with low levels of testosterone and gonadotropins consistent with congenital hypogonadotropic hypogonadism. MRI examination showed a normal pituitary and rudimentary olfactory bulbs, and formal smell testing confirmed anosmia. He exhibited no other CHH-associated phenotypes. He was diagnosed with Kallmann syndrome and testosterone therapy was initiated to develop secondary sexual characteristics. His family history is notable for hyposmia in the father (Cross-Culture Smell ID test [CC-SIT],sit score 8/12), who also carries the heterozygous *NDNF* mutation. The patient's mother and brother had normal sense of smell (mother, CC-SIT score 11/12; brother, CC-SIT score 10/12).

Family #2: *NDNF* Tyr128Thrfs*55 (heterozygous)

The Caucasian male proband was born with bilateral cryptorchidism with subsequent orchidopexy at age 2. He presented at age 13 for failure to undergo spontaneous pubertal development and no growth spurt. On examination he had prepubertal testis (testicular volume 2 ml) with low levels of testosterone and gonadotropins consistent with congenital hypogonadotropic hypogonadism. MRI examination showed bilateral olfactory bulb hypoplasia and a normal pituitary. He exhibited no other CHH-associated phenotypes except for anosmia. He was diagnosed with Kallmann syndrome and started on testosterone to develop secondary sexual characteristics. At age 16.5 years, , he had treatment withdrawal and biochemical testing confirmed persistent hypogonadotropic hypogonadism. Subsequently, he received combined gonadotropin treatment (hCG+FSH) for 2 years and his testicular volume increased to 5ml

under treatment. His parents and his sister self-report both normal smell and reproductive development, however formal smell testing and hormonal investigations were not conducted.

Family #3: *NDNF* p.Trp469* (heterozygous)

The Caucasian female was born at full term without any congenital anomalies. She first presented at age 17 for evaluation of primary amenorrhea. At that time, she exhibited some adrenarche with scant axillary hair, Tanner II pubic hair and Tanner II breast development. She was noted to be anosmic, subsequently confirmed by formal smell test (UPSIT 11/40, <5th percentile). X-rays revealed severely delayed bone age (bone age of 12 years, chronological age of 17 years) and ultrasound showed small ovaries with a small, un-estrogenized uterus. Dynamic testing demonstrated normal anterior pituitary function and serum hormone profiling indicated hypogonadotropic hypogonadism with low serum gonadotropins (LH 1.1 IU/L, FSH 0.6 IU/L) in the setting of undetectable estradiol (<30 pg/mL). The clinical and biochemical picture was consistent with Kallmann syndrome with complete absence of puberty. She was started on estrogen therapy at age 18 which induced breast development, and estro-progestins provided regular withdrawal bleeds.

At age 25 the proband underwent *in vitro* fertilization and gave birth to healthy triplets (one girl and two non-identical twin boys). The proband's daughter is normosmic (UPSIT score 38/40) and her age of menarche was 12 years. This daughter is a non-expressing carrier of the *NDNF* mutation, which is consistent with incomplete penetrance. Clinical and genetic information on the two boys is unavailable. The family history includes delayed puberty in both of the proband's brothers who also harbor the heterozygous *NDNF* mutation. Interestingly, these brothers had an apparently normal initiation of puberty, however did not complete their growth spurt until ages 25 and 28, respectively, raising the question of partial CHH in these individuals. One brother is hyposmic (UPSIT score 28/40, 6th percentile).

The proband and her brothers inherited the mutation from the father who had a low score in the formal smell test (UPSIT score 31/40, 58th percentile), however this is considered normal for his age (>70 years old at time of testing). The proband's mother has a normal sense of smell (UPSIT score 36/40), and has a normal reproductive phenotype (menarche at 14 years old).

Family #4: *NDNF* p.Thr201Ser (heterozygous)

The Caucasian male was born with micropenis and bilateral cryptorchidism for which he underwent orchidopexy at age 4. He then presented at age 16 for failure to undergo spontaneous pubertal development. He was undervirilized with modest axillary hair, eunuchoidal proportions (armspan 178cm, height of 172 cm), and prepubertal testes (1mL bilaterally). Radiologic examination revealed a delayed bone age and hormonal profiling was consistent with CHH. Based on this finding and his anosmia he was diagnosed with Kallmann syndrome and initiated testosterone replacement therapy to induce development of secondary sexual characteristics. His paternal grandfather is anosmic, consistent with familial KS.

Supplementary Figures

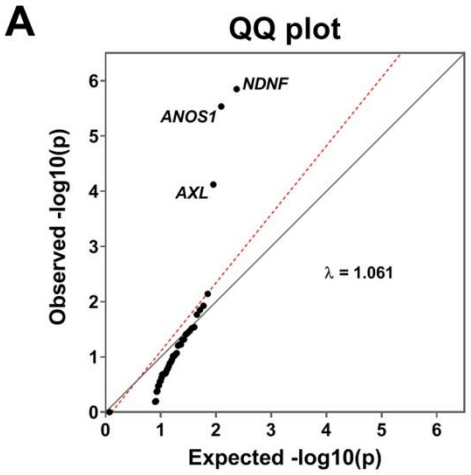

Figure S1. QQ plot illustrating the distribution of observed and expected p-values in the burden analysis of rare PTVs in FN3 genes (CHH patients versus gnomAD control database).

Supplemental Materials and Methods

Subjects, DNA sequencing and bioinformatic analysis

Centre Hospitalier Universitaire Vaudois (CHUV)

A total of 222 CHH unrelated probands (124 KS and 98 nCHH) from primarily European ancestries were included in the study. The diagnosis of CHH was determined via clinical, hormonal and radiologic evaluations as previously described [1; 2]. Additionally, in the presence of hyposmia or anosmia (either self-reported anosmia, or score <5th percentile on formal smell testing, [3; 4] Kallmann syndrome (KS) was diagnosed. When available, family members were recruited for phenotyping and genetic studies.

Whole exome sequencing (WES) was performed by BGI, Inc., Shenzhen, China. Briefly, exonic region capture using Agilent™ V2 or Agilent™ V5 and then enriched *via* library amplification. Exome capture libraries were sequenced on the Illumina™ HiSeq2000™ platform, generating .fastq paired-end files as output. The FASTQ files generated from WES were aligned in-house to the human reference sequence (UCSC GRCh37/hg19 build) using Burrows-Wheeler Aligner (BWA) algorithm, and variants were called with Genome Analysis Toolkit (GATK) [5].

Helsinki University Hospital (HUH)

Genomic DNA samples from 18 male unrelated CHH probands (15 with KS and 3 with nCHH) [6; 7] as well as one KS brother were investigated with WES. WES was provided by three different vendors (Finnish Institute of Molecular Medicine, seven samples; Axeq/Macrogen (South Korea), nine samples) as previously described [8; 9] and two samples were analyzed by Knome Inc. (US). The raw sequence data from the three WES providers were aligned in-house to the human reference sequence (UCSC GRCh37/hg19 build) using Burrows-Wheeler Aligner (BWA) algorithm. Variants were called with Genome Analysis Toolkit (GATK) [5], and visualized and analyzed with the program BasePlayer [10] .

Sanger sequencing.

The coding exons and splice junctions (≤15 bp from exon-intron boundaries) DNA sequences of *NDNF* (RefSeq NM_024574) were PCR-amplified from the genomic DNA of CHH patients. PCR products were purified with ExoSAP-IT treatment (Amersham Biosciences, Piscataway, N.J., USA), and bi-directionally sequenced using the ABI BigDyeTerminator Cycle Sequencing Kit (v3.1) and ABI Prism 3730xl DNA Analyzer automated sequencer (Applied Biosystems, Foster City, Calif., USA) by Microsynth AG, Balgach, Switzerland. Sequence variations were found on both DNA strands and were confirmed in a separate PCR. The sequences were aligned and read with Sequencher® 4.9 software (Gene Codes Corporation,

AnnArbor, Mich., USA) or Chromas Lite 2.01 (Technelysium, Australia). All primer sequences and PCR conditions are indicated below.

NDNF_Ex2F	TGTGACTTGCCTGAGTGTCTGC
NDNF_Ex2R	GCAAGCATTGCCTCCTACACG
NDNF_Ex3F	CAGATCCTTGGGGCTGTTGG
NDNF_Ex3R	TGATGCCACCCTCCCACTTC
NDNF_Ex4aF	TTGGCAAGCCACAGTGTATGCC
NDNF_Ex4aR	AAGCGGTGCTCATGTTGCTG
NDNF_Ex4bF	ACGCAGTTTCCAGGCAAAGC
NDNF_Ex4bR	CACGGTGGCTGAGGAACAGG
NDNF_Ex4cTF	TTCACTCTTGTCTGGATGCTG
NDNF_Ex4cTR	CAGGTCACAACTTCTCTCAACTG

Additional internal primer for sequencing:

NDNF_Ex3intF	CTGGTAAGTCTTGATTGTAAATGTTAG

Bioinformatic analyses.

Variants were annotated using the SnpEff (http://snpeff.sourceforge.net/) and Variant Effect Predictor (VEP) (http://www.ensembl.org/info/docs/tools/vep/index.html; last access, January 2019) tools. In addition to standard annotations, these tools provide data regarding multiple protein prediction models (PolyPhen-2 [11], SIFT [12], Mutation Taster [13], LRT, FATHMM). Genotypes were filtered to include only variants that had minor allele frequencies (MAF) of <1.0% in European controls (gnomAD, all populations).

Subjects found to harbor mutations in FN3-superfamily genes were screened by whole exome or genome sequencing for known loci underlying CHH (see list below).

Gene	OMIM #	OMIM phenotype	Report of oligogenicity
CCDC141	616031	Hypogonadotropic hypogonadism	-
CHD7	608892	CHARGE syndrome; Hypogonadotropic hypogonadism	Yes
DCC	120470	Mirror movements and/or agenesis of corpus callosum; Familial horizontal gaze palsy with progressive scoliosis (AR); Hypogonadotropic hypogonadism	-
DMXL2	612186	Polyendocrine-polyneuropathy syndrome; Autosomal dominant deafness 71	-
DUSP6	602748	Hypogonadotropic hypogonadism	-
FEZF1	613301	Hypogonadotropic hypogonadism	Yes
FGF17	603725	Hypogonadotropic hypogonadism	Yes
FGF8	600483	Hypogonadotropic hypogonadism	Yes
FGFR1	136350	Hypogonadotropic hypogonadism; Hartsfield syndrome; Jackson-Weiss syndrome; Osteoglophonic dysplasia; Pfeiffer syndrome; Trigonocephaly 1	Yes
FLRT3	604808	Hypogonadotropic hypogonadism	-
FSHB	136530	Hypogonadotropic hypogonadism	-
GNRH1	152760	Hypogonadotropic hypogonadism	Yes
GNRHR	138850	Hypogonadotropic hypogonadism	Yes
HS6ST1	604846	Hypogonadotropic hypogonadism	Yes
IGSF10	617351	Delayed puberty; Hypogonadotropic hypogonadism (?)	-
IL17RD	606807	Hypogonadotropic hypogonadism	-
KAL1	300836	Hypogonadotropic hypogonadism	Yes
KISS1	603286	Hypogonadotropic hypogonadism	Yes
KISS1R	604161	Hypogonadotropic hypogonadism; Precocious puberty (AD)	Yes
KLB	611135	Hypogonadotropic hypogonadism	-
LEP	164160	Obesity, morbid, due to leptin deficiency	Yes
LEPR	601007	Obesity, morbid, due to leptin receptor deficiency	Yes
LHB	152780	Hypogonadotropic hypogonadism	-
NR0B1	300473	Adrenal hypoplasia, congenital	-
NSMF	608137	Hypogonadotropic hypogonadism	Yes
NTN1	601614	Hypogonadotropic hypogonadism	-

OTUD4	611744	Hypogonadotropic hypogonadism	-
PCSK1	162150	Obesity with impaired prohormone processing	Yes
PLXNA1	601055	Hypogonadotropic hypogonadism	-
PNPLA6	603197	Boucher-Neuhauser syndrome; Oliver-McFarlane syndrome; Spastic paraplegia 39; Laurence-Moon syndrome	-
POLR3A	614258	Leukodystrophy hypomyelinating 7 with or without oligodontia and/or hypogonadotropic hypogonadism	-
POLR3B	614366	Leukodystrophy hypomyelinating 8 with or without oligodontia and/or hypogonadotropic hypogonadism	-
PROK2	607002	Hypogonadotropic hypogonadism	Yes
PROKR2	607123	Hypogonadotropic hypogonadism	Yes
RNF216	609948	Cerebellar ataxia and hypogonadotropic hypogonadism	-
SEMA3A	603961	Hypogonadotropic hypogonadism	Yes
SEMA3E	608166	CHARGE syndrome (possible) Hypogonadotropic hypogonadism	-
SMCHD1	614982	Bosma arhinia microphthalmia syndrome; Hypogonadotropic hypogonadism	-
SOX10	602229	PCWH syndrome; Waardenburg syndrome type 2E; Waardenburg syndrome type 4C; Hypogonadotropic hypogonadism	Yes
SOX2	184429	Syndromic microphthalmia 3 Optic nerve hypoplasia and CNS abnormalities Hypogonadotropic hypogonadism	-
SPRY4	607894	Hypogonadotropic hypogonadism	-
STUB1	607207	Spinocerebellar ataxia 16 Hypogonadotropic hypogonadism	-
TAC3	162330	Hypogonadotropic hypogonadism	Yes
TACR3	162332	Hypogonadotropic hypogonadism	Yes
TUBB3	602661	TUBB3 E410K syndrome with hypogonadotropic hypogonadism	-
WDR11	606417	Hypogonadotropic hypogonadism	Yes
AXL	109135	Hypogonadotropic hypogonadism	-

***In vitro* analysis of NDNF mutants**

Western blot.

Sub-confluent COS7 cells in 24-well plates were transiently transfected with 5 ng or 100 ng of flag-tagged WT or mutant NDNF for analysis of cell lysate and secreted protein levels respectively, using FuGene HD reagent (Roche Diagnostics). Following a 16 h incubation in a full growth medium, the medium was changed to a reduced serum medium (OptiMEM, Life Technology) and the cells were incubated for an additional 24 h. Equal amounts of WT and mutant cleared lysate (5-10 μg of total protein) and 20 ul of cleared conditioned medium were resolved on NuPAGE 10% Bis-Tris gels (Life Technologies) under reducing conditions and then subjected to Western blot analysis using an anti-flag primary antibody (M2 clone, Sigma-Aldrich) and goat anti-mouse horseradish peroxidase-conjugated secondary antibody (Upstate Biotechnology). Blots were stripped using Restore Western Blot Stripping Buffer (Pierce) and re-probed with horseradish peroxidase-conjugated anti-β-actin antibody (Abcam, Cambridge, MA). Flag-NDNF and β-actin immunoreactivity were quantified by densitometry (ImagJ software). Specific NDNF expression levels were normalized to the expression levels of β-actin and reported as a ratio to WT. For analysis of conditioned medium experiments, we measured the NDNF migrating band at an expected molecular weight (Thr201Ser, ~75 kD; Trp463* ~60kD). Experiments were repeated 5 times, and protein expression levels were compared between each mutant and WT protein using Student's t-test. Data are presented as mean ± SEM.

Cell-surface expression.

Sub-confluent COS7 cells were transfected with WT or mutant NDNF plasmids. After 24 h the cells were rinsed and incubated at room temperature for 3-4 h in binding buffer (50 mM Tris-HCl, 100 mM NaCl, 5 mM KCl, 2 mM $CaCl_2$, 5% heat-inactivated horse serum, 0.5% fetal bovine serum, pH 7.7) containing anti-FLAG antibody (1:1500, M2 clone, Sigma-Aldrich). Cells were then rinsed and incubated at room

temperature for 2 h in binding buffer containing [^{125}I]-rabbit anti-mouse IgG (300,000 cpm/well; PerkinElmer), prior to being lysed in 1 N NaOH. The radioactivity in the lysates was measured via gamma-counter, and experiments were performed in quadruplicate. Results were expressed as percent WT, and the mean specific expression levels of WT and mutant NDNF from 4 independent experiments were compared using ANOVA followed by Dunnett's correction for multiple comparisons.

Reporter gene assay.

To detect activation of the PLCγ/Ca^{+2} cascade downstream of FGF8/FGFR1 we used the nuclear factor of activated T-cells (NFAT)-luciferase reporter (addgene plasmid 10959; Ichida, M. and Finkel, T. 2001 *J Biol Chem*, 276; [14; 15]. COS7 cells were transiently transfected with 75ng NFAT-Luc reporter together with 5ng FGFR1, 10ng WT or mutant NDNF expression plasmids, and 110ng pCDNA3.1 empty vector using FuGENE HD reagent (Promega). Following a 16h incubation in full growth medium, cells were starved in serum free medium for 8h and then stimulated overnight with increasing doses (0-50 nM) of FGF8 (provided by Dr. M. Mohammadi). Assays were preformed in triplicate and repeated at least 3 times. Reporter activation levels of WT and mutant NDNF from each experiment were expressed as a percent of the maximal FGF8 dose response obtained in the absence of NDNF, and the mean values from 3 independent experiments were fitted using a three-parameter sigmoidal curve (Prism6, GraphPad Software). Response at the highest dose of mutant NDNF was compared to that of WT using ANOVA followed by Dunnett's correction for multiple comparisons.

Production and purification of human recombinant NDNF

Full-length untagged 568 aa recombinant human NDNF protein (Uniprot Q8TB73) was produced using the QMCF stable episomal expression system following cDNA codon optimization in CHO cells by Icosagen,

Estonia. Purification of secreted recombinant NDNF from CHO culture medium was performed by denaturation with 3M urea followed by HiTrap SP HP cation exchange chromatography. Protein was eluted with 20 mM Na-phosphate pH 7.0 with 2 M NaCl. Eluted protein was further purified by gel filtration with Superdex 200 Increase 10/300 column followed by buffer exchange into the PBS (pH 7,4), 0.7M NaCl. Product was concentrated to 1 mg/ml by Amicon concentrator, and protein concentration was verified by Nanodrop (Ext coef. 46.6).

In vivo zebrafish model

Zebrafish strains and treatments.

Morpholinos sequences for NDNF (wu:fb16h09):

zFB16-SS	CTGGCTCACCTAAGACACAGGAAAC
zFB16-ATG	ATAACATCCACACCTCCACGTCATC

Control MO sequence:

5' TCGTGGCCATCAACTCGAACA 3'

NDNF expression studies

Fluorescence-activated cell sorting and gene expression analysis.

Embryos were harvested at E14.5 and E18.5 from timed-pregnant GnRH-GFP mice anesthetized with an i.p. injection of 100 mg/kg of ketamine-HCl and sacrificed by cervical dislocation. Microdissected tissues were enzymatically dissociated using the Papain Dissociation System (Worthington, Lakewood, NJ) to obtain single-cell suspensions as previously described [16]. After dissociation, the cells were physically purified using a FACSAria III (Beckman Coulter) flow cytometer equipped with FACSDiva software (BD

Biosciences). The sort decision was based on measurements of GFP fluorescence (excitation: 488nm, 50 mW; detection: GFP bandpass 530/30 nm, autofluorescence bandpass 695/40nm) by comparing cell suspensions from GnRH-GFP and wild-type animals. For each animal, 500 GFP-positive cells and 500 GFP-negative cells were sorted directly into 8µl of extraction buffer: 0.1% Triton X-100 (Sigma-Aldrich) and 0.4 U/µl RNaseOUT™ (Life Technologies). Captured cells were used to synthesize first-strand cDNA using the SuperScript III First-Strand Synthesis System for reverse transcription (RT)-PCR (Invitrogen) following the manufacturer's instructions. Controls without reverse transcriptase were performed to demonstrate the absence of contaminating genomic DNA. We used SuperScript® III Reverse Transcriptase (Life Technologies) and a linear preamplification step was performed using the TaqMan® PreAmp Master Mix Kit protocol (Applied Biosystems). Real-time PCR was carried out on Applied Biosystems 7900HT Fast Real-Time PCR System using exon-boundary-specific TaqMan® Gene Expression Assays (Applied Biosystems): *Gnrh1* (Mm01315605_m1), *NDNF* (Mm00549567_m1), *Actin* (Mm00607939_s1), *Rn18S* (Mm04277571_s1). Quantitative real-time PCR was performed using TaqMan Low-Density Arrays (Applied BioSystems) on an Applied BioSystems 7900HT thermocycler using the manufacturer's recommended cycling conditions. Gene expression data were analyzed using SDS 2.4.1 and Data Assist 3.0.1 software (Applied BioSystems). Data were compared by one-way ANOVA for multiple comparisons followed by Tukey's least significant difference post hoc test. The significance level was set at $p < 0.05$ in all cases. Data are represented by means ± SEM.

Ndnf knock-out mice

Genotyping of the mice was performed with DNA isolated from ear samples or from decapitated mouse embryos with Macherey-Nagel NucleoSpin Tissue kit according to manufacturer's instructions.

Genotyping was performed by PCR and agarose gel electrophoresis. Primers used in genotyping are shown in the table below.

Reaction	Primer name	Primer sequence	Product size
PCR to detect mutant allele	KO_Ndnf_Fw	5' ACAATTGTTCACTCTGCTCACCAG 3'	300 bp
	KO_Ndnf_Rv	5' TCGTGGTATCGTTATGCGCC 3'	
PCR to detect wild type allele	WT_Ndnf_Fw	5' GACTTCCTTTGTACTGTCTTGGG 3'	675 bp
	WT_Ndnf_Rv	5' TGTGCCCTCTACATCAGTCA 3'	

iDISCO whole-mount staining

Experiments were performed as previously described (Renier et al., Cell 2014) and detailed below.

Sample pre-treatment with methanol

Samples were washed in PBS (twice for 1h), followed by 50% methanol in PBS (once for 1h), 80% methanol (once for 1h) and 100% methanol (twice for 1h). Next, samples were bleached in 5% H_2O_2 in 20% DMSO/methanol (2ml 30% H_2O_2/2ml DMSO/8ml methanol, ice cold) at 4°C overnight. Next, samples were washed in methanol (twice for 1h), in 20% DMSO/methanol (twice for 1h), 80% methanol (once for 1h), 50% methanol (once for 1h), PBS (twice for 1h), and finally, PBS/0.2% TritonX-100 (twice for 1h) before proceeding to the staining procedures.

Samples were incubated at 37°C on an adjustable rotator in 10 ml of a blocking solution (PBSGNaT) of 1X PBS containing 0.2% gelatin (Sigma), 0.5% Triton X-100 (Sigma-Aldrich) and 0.01% NaAzide for 3 nights. Samples were transferred to 10 ml of PBSGNaT containing primary antibodies (see *GnRH cell counting* for details) and placed at 37°C in rotation for 7 days. This was followed by six washes of 30min in PBSGT at RT and a final wash in PBSGT overnight at 4°C. Next, samples were incubated in secondary antibodies

(1:400, Alexa 568, Alexa 647) diluted in 10 ml PBSGNaT for 2 days at 37°C in a rotating tube. After six 30-min washes in PBS at room temperature, the samples were stored in PBS at 4°C in the dark until clearing.

Tissue clearing

All incubation steps were performed at RT in a fume hood on a tube rotator at 14 rpm covered with aluminium foil to avoid contact with light. Samples were dehydrated in a graded series (50%, 80%, and 100%) of tetrahydrofurane (THF; anhydrous, containing 250 ppm butylated hydroxytoluene inhibitor, Sigma-Aldrich) diluted in H2O as follow: 1) 50% THF overnight at RT; 2) 80% THF 1h at RT; 3) 100% THF 1h30 at RT; 4) 100% THF 1h30 at RT. This was followed by a delipidation step of 30-40 min in 100 % dichloromethane (DCM; Sigma-Aldrich). Samples were cleared in dibenzylether (DBE; Sigma-Aldrich) for 2h at RT on constant agitation and in the dark. Finally, samples were moved into fresh DBE and stored in glass tubes in the dark and at RT until imaging. We could image samples, as described below, without any significant fluorescence loss for up to 6 months.

Imaging

3D imaging was performed as previously described (Belle et al., 2014) using an ultramicroscope (LaVisionBioTec) with ImspectorPro software (LaVisionBioTec). The light sheet was generated by a laser (wavelength 488 or 561 nm, Coherent Sapphire Laser, LaVisionBioTec) and two cylindrical lenses. A binocular stereomicroscope (MXV10, Olympus) with a 2× and 4x objective (MVPLAPO, Olympus) was used at different magnifications (1.6×, 4×, 5×, and 6.3×). Samples were placed in an imaging reservoir made of 100% quartz (LaVisionBioTec) filled with DBE and illuminated from the side by the laser light. A PCO Edge SCMOS CCD camera (2560 × 2160 pixel size, LaVisionBioTec) was used to acquire images. The step size between each image was fixed at 2 µm.

Image analysis

For confocal observations and analyses, an inverted laser scanning Axio observer microscope (LSM 710, Zeiss, Oberkochen, Germany) with EC Plan NeoFluor 10×/0.3 NA, 20×/0.5 NA and 40×/1.3 NA (Zeiss, Oberkochen, Germany) objectives were used (Imaging Core Facility of IFR114 of the University of Lille, France).

Images, 3D volume, and movies were generated using Imaris x64 software (version 7.6.1, Bitplane). Stack images were first converted to imaris file (.ims) using ImarisFileConverter and 3D recontruction was performed using "volume rendering". Optical slices of samples were obtained using the "orthoslicer" tools. The surface of the samples was created using the "surface" tool by creating a mask around each volume. The peripherin-positive fibers and GnRH neurons were segmented to allow easier visualization and comparison between samples. 3D pictures were generated using the "snapshot" tool. ImageJ (National Institute of Health, Bethesda, USA) and Photoshop CS6 (Adobe Systems, San Jose, CA, USA) were used to process, adjust and merge the photomontages. Figures were prepared using Adobe Photoshop and Abode Illustrator CS6.

Supplemental references

1. Pitteloud, N., Hayes, F.J., Boepple, P.A., DeCruz, S., Seminara, S.B., MacLaughlin, D.T., and Crowley, W.F., Jr. (2002). The role of prior pubertal development, biochemical markers of testicular maturation, and genetics in elucidating the phenotypic heterogeneity of idiopathic hypogonadotropic hypogonadism. J Clin Endocrinol Metab 87, 152-160.
2. Pitteloud, N., Hayes, F.J., Dwyer, A., Boepple, P.A., Lee, H., and Crowley, W.F., Jr. (2002). Predictors of outcome of long-term GnRH therapy in men with idiopathic hypogonadotropic hypogonadism. J Clin Endocrinol Metab 87, 4128-4136.
3. Doty, R.L., Shaman, P., Kimmelman, C.P., and Dann, M.S. (1984). University of Pennsylvania Smell Identification Test: a rapid quantitative olfactory function test for the clinic. Laryngoscope 94, 176-178.
4. Doty, R.L., Marcus, A., and Lee, W.W. (1996). Development of the 12-item Cross-Cultural Smell Identification Test (CC-SIT). Laryngoscope 106, 353-356.
5. McKenna, A., Hanna, M., Banks, E., Sivachenko, A., Cibulskis, K., Kernytsky, A., Garimella, K., Altshuler, D., Gabriel, S., Daly, M., et al. (2010). The Genome Analysis Toolkit: a MapReduce framework for analyzing next-generation DNA sequencing data. Genome Res 20, 1297-1303.
6. Laitinen, E.M., Vaaralahti, K., Tommiska, J., Eklund, E., Tervaniemi, M., Valanne, L., and Raivio, T. (2011). Incidence, phenotypic features and molecular genetics of Kallmann syndrome in Finland. Orphanet J Rare Dis 6, 41.
7. Laitinen, E.M., Tommiska, J., Sane, T., Vaaralahti, K., Toppari, J., and Raivio, T. (2012). Reversible congenital hypogonadotropic hypogonadism in patients with CHD7, FGFR1 or GNRHR mutations. PloS one 7, e39450.
8. Sulonen, A.M., Ellonen, P., Almusa, H., Lepisto, M., Eldfors, S., Hannula, S., Miettinen, T., Tyynismaa, H., Salo, P., Heckman, C., et al. (2011). Comparison of solution-based exome capture methods for next generation sequencing. Genome Biol 12, R94.
9. Palmio, J., Evila, A., Chapon, F., Tasca, G., Xiang, F., Bradvik, B., Eymard, B., Echaniz-Laguna, A., Laporte, J., Karppa, M., et al. (2014). Hereditary myopathy with early respiratory failure: occurrence in various populations. J Neurol Neurosurg Psychiatry 85, 345-353.
10. Katainen, R., Donner, I., Cajuso, T., Kaasinen, E., Palin, K., Makinen, V., Aaltonen, L.A., and Pitkanen, E. (2018). Discovery of potential causative mutations in human coding and noncoding genome with the interactive software BasePlayer. Nat Protoc 13, 2580-2600.
11. Adzhubei, I.A., Schmidt, S., Peshkin, L., Ramensky, V.E., Gerasimova, A., Bork, P., Kondrashov, A.S., and Sunyaev, S.R. (2010). A method and server for predicting damaging missense mutations. Nature methods 7, 248-249.
12. Kumar, P., Henikoff, S., and Ng, P.C. (2009). Predicting the effects of coding non-synonymous variants on protein function using the SIFT algorithm. Nature protocols 4, 1073-1081.
13. Schwarz, J.M., Rodelsperger, C., Schuelke, M., and Seelow, D. (2010). MutationTaster evaluates disease-causing potential of sequence alterations. Nature methods 7, 575-576.
14. Ichida, M., and Finkel, T. (2001). Ras regulates NFAT3 activity in cardiac myocytes. J Biol Chem 276, 3524-3530.
15. Crabtree, G.R., and Olson, E.N. (2002). NFAT signaling: choreographing the social lives of cells. Cell 109 Suppl, S67-79.
16. Giacobini, P., Parkash, J., Campagne, C., Messina, A., Casoni, F., Vanacker, C., Langlet, F., Hobo, B., Cagnoni, G., Gallet, S., et al. (2014). Brain Endothelial Cells Control Fertility through Ovarian-Steroid-Dependent Release of Semaphorin 3A. PLoS biology 12, e1001808.